DUDLEY KNOX LIBRARY
NAVAL POSTGRADUATE SCHOOL
MONTEREY, CALIFORNIA 93943-5002

NAVAL POSTGRADUATE SCHOOL
Monterey, California

THESIS

AN EVALUATION OF THE IMPACT
OF VARIABLE TEMPORAL AND SPATIAL
DATA RESOLUTION UPON IREPS

by

Michael E. Dotson

June 1987

Co-Advisor W. J. Shaw
Co-Advisor D. W. Thomson

Approved for public release; distribution is unlimited.

T234161

REPORT DOCUMENTATION PAGE

1a REPORT SECURITY CLASSIFICATION UNCLASSIFIED	1b RESTRICTIVE MARKINGS
2a SECURITY CLASSIFICATION AUTHORITY	3 DISTRIBUTION / AVAILABILITY OF REPORT Approved for public release; distribution is unlimited.
2b DECLASSIFICATION / DOWNGRADING SCHEDULE	
4 PERFORMING ORGANIZATION REPORT NUMBER(S)	5 MONITORING ORGANIZATION REPORT NUMBER(S)
6a NAME OF PERFORMING ORGANIZATION Naval Postgraduate School 6b OFFICE SYMBOL (If applicable) 63	7a NAME OF MONITORING ORGANIZATION Naval Postgraduate School
6c ADDRESS (City, State, and ZIP Code) Monterey, California 93943-5000	7b ADDRESS (City, State, and ZIP Code) Monterey, California 93943-5000
8a NAME OF FUNDING / SPONSORING ORGANIZATION 8b OFFICE SYMBOL (If applicable)	9 PROCUREMENT INSTRUMENT IDENTIFICATION NUMBER
8c ADDRESS (City, State, and ZIP Code)	10 SOURCE OF FUNDING NUMBERS PROGRAM ELEMENT NO / PROJECT NO / TASK NO / WORK UNIT ACCESSION NO

11 TITLE (Include Security Classification)
AN EVALUATION OF THE IMPACT OF VARIABLE TEMPORAL AND SPATIAL DATA RESOLUTION UPON IREPS

12 PERSONAL AUTHOR(S)
Dotson, Michael E.

13a TYPE OF REPORT	13b TIME COVERED	14 DATE OF REPORT (Year, Month, Day)	15 PAGE COUNT
Master's Thesis	FROM _____ TO _____	1987 June	63

16 SUPPLEMENTARY NOTATION

17 COSATI CODES			18 SUBJECT TERMS (Continue on reverse if necessary and identify by block number)
FIELD	GROUP	SUB-GROUP	Atmospheric Refractivity, IREPS, EM Systems Performance, Horizontally Homogeneous Atmosphere, Refractive Index

19 ABSTRACT (Continue on reverse if necessary and identify by block number)

Atmospheric refractive index gradients significantly modify the path of electro-magnetic (EM) waves as they propagate through the atmosphere. Accordingly, the performance of U.S. Navy (EM) systems can be either degraded or enhanced due to atmospheric conditions which affect atmospheric refractive index profiles. The Integrated Refractive Effects Prediction System (IREPS) version 2.2 is the latest software developed by Naval Ocean Systems Center (NOSC) to predict atmospheric refraction and its resulting effect on EM systems. Specific environmental parameters are used as input data to produce various output products to be used by the tactician in planning the optimum use of naval assets. As with any model, the quality and accuracy of the resulting output is directly related to the quality and timeliness of the input data. This thesis study shows the importance of timely, high

20 DISTRIBUTION / AVAILABILITY OF ABSTRACT	21 ABSTRACT SECURITY CLASSIFICATION
☒ UNCLASSIFIED/UNLIMITED ☐ SAME AS RPT ☐ DTIC USERS	UNCLASSIFIED
22a NAME OF RESPONSIBLE INDIVIDUAL Prof. W.J. Shaw	22b TELEPHONE (Include Area Code) (804) 646-3430 / 22c OFFICE SYMBOL Code 63Sr

DD FORM 1473, 84 MAR 83 APR edition may be used until exhausted
All other editions are obsolete

resolution data, for input into the IREPS version 2.2 program, in order to obtain realistic atmospheric refractive and corresponding EM system performance predictions. A continentally derived data set is used to compare the results of using high resolution versus low resolution data as input into IREPS, and to qualitatively show how quickly the refractive structure of the atmosphere can vary with time. A second data set from an over ocean experiment attacks the horizontally homogeneous atmosphere assumption which appears to be frequently incorrectly applied. Finally, a statistical comparison is performed to evaluate the extent to which the natural variability of the atmosphere can result in significant variations of atmospheric refractivity that could affect naval EM systems.

Approved for public release; distribution is unlimited.

An Evaluation of the Impact of Variable Temporal and Spatial Data Resolution upon IREPS

by

Michael E. Dotson
Lieutenant, United States Navy
B.S., United States Naval Academy,1981

Submitted in partial fulfillment of the
requirements for the degree of

MASTER OF SCIENCE IN METEOROLOGY AND OCEANOGRAPHY

from the

NAVAL POSTGRADUATE SCHOOL
June 1987

Thesis
D6643
c.1

ABSTRACT

Atmospheric refractive index gradients significantly modify the path of electromagnetic (EM) waves as they propagate through the atmosphere. Accordingly, the performance of U.S. Navy (EM) systems can be either degraded or enhanced due to atmospheric conditions which affect atmospheric refractive index profiles. The Integrated Refractive Effects Prediction System (IREPS) version 2.2 is the latest software developed by Naval Ocean Systems Center (NOSC) to predict atmospheric refraction and its resulting effect on EM systems. Specific environmental parameters are used as input data to produce various output products to be used by the tactician in planning the optimum use of naval assets. As with any model, the quality and accuracy of the resulting output is directly related to the quality and timeliness of the input data. This thesis study shows the importance of timely, high resolution data, for input into the IREPS version 2.2 program, in order to obtain realistic atmospheric refractive and corresponding EM system performance predictions. A continentally derived data set is used to compare the results of using high resolution versus low resolution data as input into IREPS, and to qualitatively show how quickly the refractive structure of the atmosphere can vary with time. A second data set from an over ocean experiment attacks the horizontally homogeneous atmosphere assumption which appears to be frequently incorrectly applied. Finally, a statistical comparison is performed to evaluate the extent to which the natural variability of the atmosphere can result in significant variations of atmospheric refractivity that could affect naval EM systems.

TABLE OF CONTENTS

LIST OF TABLES

LIST OF FIGURES

ACKNOWLEDGEMENTS

This thesis study project was suggested by Dr. D.W. Thomson of the Department of Meteorology at the Pennsylvania State University while he was serving as the NAVAIR G.J. Haltiner research chair professor at the Naval Postgraduate School (NPS). For their knowledge, guidance, support and patience, I want to extend my sincere appreciation to him as well as my co-advisor, Professor W.J. Shaw (NPS).

The scrutiny and analysis by AG2 Marty Schy of 120 sounding profiles is gratefully acknowledeged. Mike Gunning provided the useful skew T-log P plotting routine. The IREPS programs were run at the Naval Environmental Prediction Research Facility (NEPRF) with the able assistance of John Cook and his computer wizard associates. I would also like to thank Chris Vaucher for the use of his figures, and Ann for her constant support and her random number generating abilities.

This research was made possible in part by funding from NEPRF, Monterey, Ca. under program element 62435N, project R3581 "System Environmental Sensitivity".

I. INTRODUCTION

The Atmospheric Boundary Layer (ABL) is defined by Stewart (1979) as that portion of the lower atmosphere which has turbulent flow and is in direct contact with the earth's surface. The ABL extends from the earth's surface to a height of several ten's to thousands of meters. All momentum, water vapor, and thermal energy exchanges between the atmosphere and the earth's surface take place within the ABL. The stability of the ABL is dependent upon its density structure. The density structure in turn is a function of water vapor distribution and whether the layer is heated or cooled from below. While both stable and unstable ABLs have some energy for vertical mixing as a result of shear production of turbulent kinetic energy (TKE), when there is heating from the earth's surface, the heating produces a density distribution which enhances vertical mixing. In this unstable case, the overall level of TKE, and hence vertical mixing, is greater. The unstably statified boundary layer layer can be further subdivided into three separate layers: the surface layer, the mixed layer, and a capping inversion layer.

For the near-neutral to unstable case, depending upon the magnitude and direction of the thermal energy flux, the depth of the surface layer typically ranges from a few meters to several ten's of meters, and is conventionally considered to occupy the lower tenth of the ABL (Wyngaard, 1973). Physical continuity between the atmosphere and the earth dictates that wind velocity be zero at the immediate surface over land and equal to the surface drift current over water. Above the surface, velocity increases in approximately a logarithmic fashion to the top of the layer. Thus, strong vertical wind shear is common in this layer. It, along with convection, produces turbulence which facilitates the transport of moisture and momentum within the layer. The relatively homogeneous mixed layer directly above the turbulent surface layer constitutes the majority of the unstable ABL. Turbulence tends to continuously erode local gradients and, thus, conditions are well-mixed up to the inversion layer. The last 50 to 100 meters of the convective ABL is usually an inversion layer. In it the kinetic energy available for mixing is damped by strong stable vertical temperature gradients. The gradients have a "capping" effect on the convection below and effectively suppress exchange of physical properties with the free atmosphere above.

If the ABL is cooled from below it will be stable. Turbulence is suppressed by the resulting density structure, and generally little mixing will occur except in the surface layer. All exchanges between the atmosphere and the earth's surface are thus greatly reduced.

It is in the marine atmospheric boundary layer (MABL) that the oceans and the atmosphere exchange energy directly in the form of turbulent heat, moisture and momentum fluxes. Gases and solids are also in continuous exchange between each fluid. Wave activity can toss small water droplets directly into the lower atmosphere where they become suspended and eventually evaporate. Normally, evaporation from the sea surface creates a shallow layer of rapidly decreasing relative humidity from 100% at the sea surface to a lower value (80-90%) directly above the sea surface. This low level feature produces an extended radar propagation phenomenon known as an evaporation duct because of its formation mechanism. The evaporation duct extends only tens of meters above the ocean's surface but is of great importance to the mariner because it occurs in varying degrees throughout all oceanic areas and results in over-the-horizon radar propagation.

The ABL over land shows much more variation than the MABL. Seasonal and diurnal changes are both more pronounced. Larger variations in the vertical temperature structure occur over land than over the ocean but there is usually less vertical humidity variation. Radiative heating and cooling can cause large diurnal fluctuations in the height of the ABL from near surface values at night to over 2000 meters during the day.

Propagating electromagnetic (EM) waves, unless in a completely homogeneous medium, will experience some degree of bending due to changes in the index of refraction. The earth's atmosphere is normally a very inhomogeneous fluid. Certain regions such as the ABL characteristically have large mean gradients in temperature and or humidity. Rapid vertical changes in both temperature and humidity create layers which significantly refract propagating EM signals. This phenomenon is readily apparent, for example, in the evaporation duct at the base of the MABL and in the inversion layer at the top of the ABL. Refraction of EM waves will receive more detailed discussion in Chapter two.

The Integrated Refractive Effects Prediction System (IREPS) is a shipboard environmental data processing and display system which is used to predict the effects of refraction on electromagnetic signals for naval surveillance, communications,

electronic warfare, and weapons guidance systems. Environmental data usually obtained from radiosondes are processed on a desk top computer, the Hewlett-Packard 9845, to derive a comprehensive assessment of refractive effects in the lower atmosphere. Knowledge of the refractive environment can be used to maximize tactical advantage. The most recent IREPS, version 2.2, is presently scheduled to be an integral part of the Tactical Environmental Support System (TESS)(NOSC TD 659, 1981), soon to be introduced into the fleet.

The performance of the IREPS model is directly related to the quality and timeliness of atmospheric information entered into the program. Accurate and timely data must be used if the resulting coverage displays are to indicate the true refractive structure of the atmosphere. Knowledge of the immediate environment and its dynamical evolution are necessary for a proper interpretation of IREPS results. The IREPS revision 2.2 User's Manual on page 49 (NOSC TD 659, 1981) states that the assumption of a horizontally homogeneous atmosphere is valid about 85 percent of the time for the purpose of making refractive effects assessments. Given the natural variability evident in atmospheric soundings made with measurement systems having high temporal resolution (e.g. Webb, 1977), this statement may be too optimistic. Thus, one of the objectives of this thesis is to examine the validity of the assumption of the horizontally homogeneous atmosphere. By selecting a data set in an oceanic area which was previously believed to be homogeneous, we investigate how the vertical structure of the immediate atmosphere controls the nature of radar propagation. We are concerned not only with the spatial variability of the atmosphere, but also its temporal variability. The atmosphere undergoes continous dynamic evolution in diurnal as well as synoptic time scales. The IREPS User's Manual notes that "the user should be aware of the changing state of the atmosphere and try to acquire and use refractivity measurements that are appropriate to the planned time and place of pertinent operations." Our second objective is to attempt to qualitatively determine the length of time an IREPS product could remain an operationally useful predictor of the refractive structure of the surrounding environment. Thirdly, we expect that in order to derive an accurate IREPS assessment of the refractive structure of the atmosphere, high vertical resolution data are required. Presumably, unless the vertical resolution of the input data is sufficient to define relatively thin layers of strong temperature and humidity gradients which could affect atmospheric refractivity (e.g. the inversion layer of an ABL), the resulting IREPS output will not be an accurate representation of the

actual atmospheric refractive structure. Accordingly, the differences in IREPS output products, depending solely upon the quality of resolution of the input data, will be compared.

The FORTRAN code used in TESS was used to run various IREPS products at the Naval Environmental Research Prediction Facility (NEPRF). Although TESS is not yet operational, the newest revision of the IREPS code, version 2.2, was used for all the atmospheric refraction computations. Thus, the results of this work should be directly applicable to any naval unit depending upon TESS for atmospheric structure and refractive effects information.

II. ATMOSPHERIC REFRACTIVITY

The index of refraction of a medium, n, is defined by (2.1) where c is the velocity of an EM wave in free space and v is the velocity of the same EM wave in the medium.

$$n = c/v \tag{2.1}$$

For the atmosphere, the refractive index is defined to be the ratio of the velocity of propagation of an EM wave in a free space to that in the air. Since the velocity of an EM wave in a free space is always faster than that in any medium, the index of refraction is always greater than one. In the standard atmosphere, a typical near sea level value for n is approximately 1.0003 (Bean and Dutton, 1966). For convenience, the refractivity N is defined (2.2) such that normal atmospheric values of N units range from 250 to 400.

$$N = (n - 1) * 10^6 \tag{2.2}$$

As stated by Battan (1973), "In dry air the index of refraction has the same value over almost the entire range of the electromagnetic spectrum: it is the same for light and radio waves. However, when water vapor is added to the air, the value of N for the mixture becomes frequency dependent. It is well known the water molecule is polar in nature and that the dipole moment of the molecule has a different response to different-frequency radio waves. With the extremely high frequencies of visible light, the water molecules are electronically polarized. With the lower frequencies of radar waves, the water molecules not only acquire electronic polarization, but also reorient themselves rapidly enough to follow the electric-field changes. As a result, the index of refraction (and dielectric constant) of water vapor is greater for radio than for optical frequencies." Temperature, water vapor and pressure are the major variables of the atmosphere which determine its refractivity. Bean and Dutton (1966) express refractivity in terms of temperature T in Kelvins, with pressure P and water vapor pressure e in mb as follows in (2.3):

$$N = 77.6\ P/T - 5.6\ e/T + 3.75 * 10^5\ e/T^2 \tag{2.3}$$

In an atmosphere of constant N units, no bending of an EM wave could occur regardless of the value of N. EM refraction is dependent upon the gradients of N. Since gradients of pressure, temperature and humidity occur throughout the atmosphere, it follows that gradients of N must also exist. It can be shown (Battan, 1973) that when the gradient of N (i.e. dN/dz) is equal to -157 Km^{-1}, a propagating EM wave will bend with a curvature exactly equal to that of the earth. This would cause a horizontally propagating EM wave to remain constantly parallel to the earth's surface always at the same height. Any value of dN/dz less than -157 Km^{-1} would cause an EM wave to bend with greater curvature than the earth's surface. Therefore, -157 Km^{-1} is the threshold for trapping of an EM wave.

It is sometimes convenient to portray the earth's surface as being flat and to present the refraction of an EM wave in this frame of reference. This can be done simply by mathematically subtracting the earth's curvature from the EM wave and the earth. A modified index of refraction, M, is derived on this basis. It is often used in vertical profiles to provide a direct indication of refracting conditions that would cause an EM wave to bend either toward or away from the earth's surface. (2.4) (after Battan, 1973) relates the modified index of refraction at any height to the refractivity at that height.

$$M = N + 157z \qquad (2.4)$$

In vertical displays of the modified refractivity, any layer where M decreases with increasing height (a negative value of dM/dz) is an indication of a region where an EM wave would bend with a curvature greater than that of the earth. Depending on the height, strength and extent of this type of layer, an EM wave could be refracted into the earth's surface. Subsequent reflections would direct this EM wave back into the atmosphere such that over-the-horizon radar ranges can result. This is the characteristic of an evaporation duct which makes it so important in naval operations. Elevated trapping layers, too, can result in extended radar ranges. However, depending upon the height of the particular layer, this form of ducting may be of more importance to airborne radar system than to surface based units. Fig. 2.1 portrays the basic types of ducting that may occur due to typical M vertical profiles.

Profile (a) of Fig. 2.1 depicts an elevated duct which is the type often found in an inversion layer. This type of ducting condition can occur when warm, dry air exists

over a layer of cooler, moist air. This phenomenon is particulary pronounced over regions in eastern oceans and to a lesser degree in regions with trade wind inversions. The top of the duct is defined as the height where M reaches its minimum value. The thickness of the duct is found by dropping a vertical line from the top of the duct down towards the surface until the M profile is again intersected. Duct strength is defined as the maximum range of M values within the limits of the duct. The optimum coupling height (OCH) is the height where the dM/dZ profile changes from a positive to a negative value. Profile (b) is an example of a surfaced-based duct. These ducts can be formed by warm, dry air being advected over a cool body of water, or by strong subsidence modifying an elevated duct. Profile (c) typically occurs as the result of an evaporation duct over a body of water. Over land this type of M profile is common during the summer when nocturnal radiation over moist ground leads to a temperature inversion and a rapid decrease in moisture with height (Battan, 1973). Both profiles (b) and (c) are of direct concern to the mariner whose radar antennas are frequently found within the limits of these ducts.

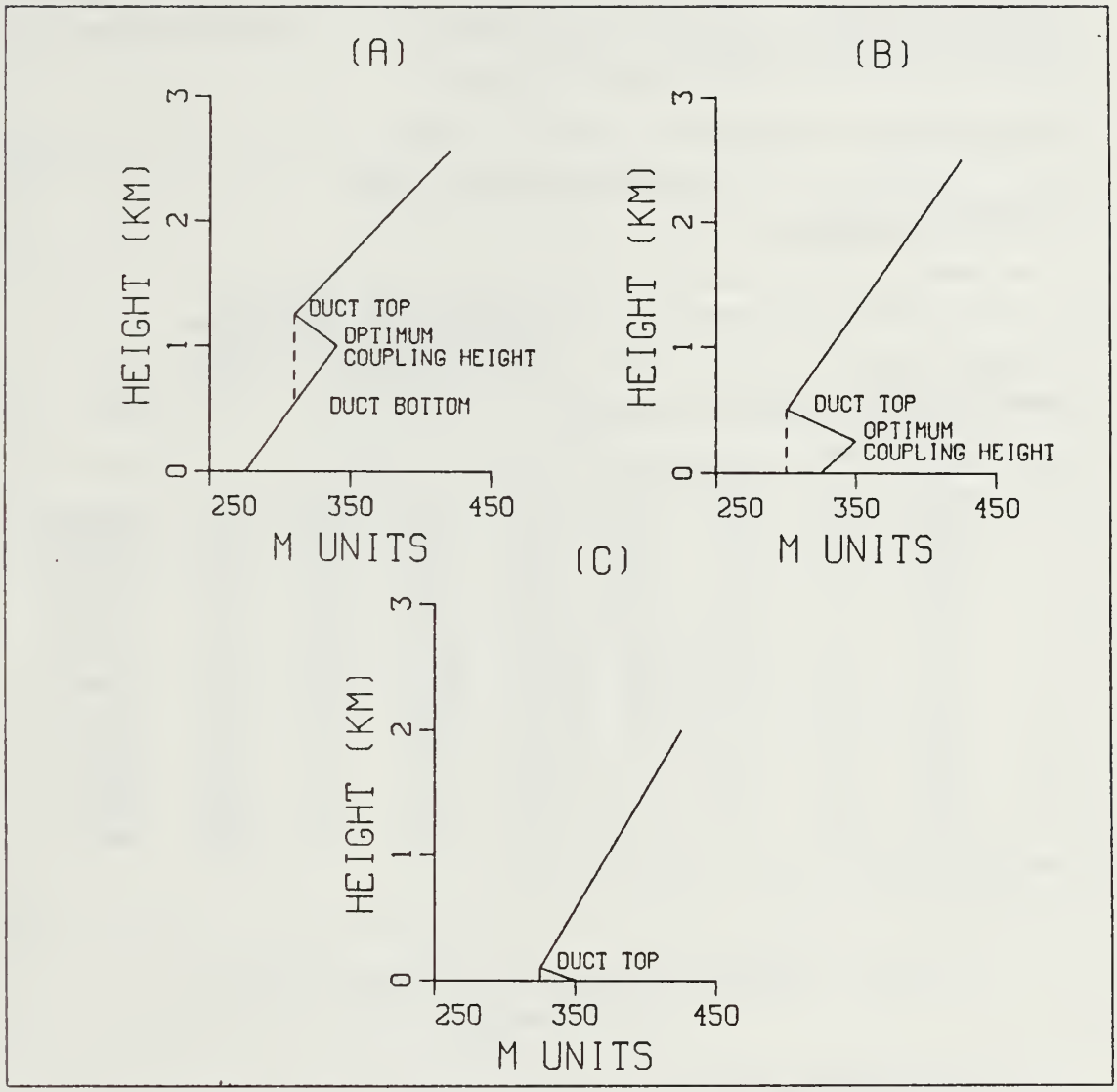

Fig. 2.1 Ducting occurrences for typical M profiles.

III. DESCRIPTION OF SOME IREPS OUTPUT PRODUCTS

Fig. 3.1 is a representation of one type of IREPS product. The "environmental data list" is used primarily for checking the numerical values of the input data. The IREPS computed output values of dew-point depression, dN/dz values, M units and a single word description of the refractive conditions give an overall assesment of the atmospheric refractive conditions at each input level.

IREPS REV 2.2

**** ENVIRONMENTAL DATA LIST ****

LOCATION: FASINEX
DATE/TIME: ENDEAVOR #1

WIND SPEED 7.1 METRES PER SECOND

EVAPORATION DUCT PARAMETERS:
SEA TEMPERATURE 21.01 DEGREES C
AIR TEMPERATURE 18.8 DEGREES C
RELATIVE HUMIDITY 73.8 PERCENT
EVAPORATION DUCT HEIGHT 15.4 METRES

SURFACE PRESSURE = 1026.2 mB
RADIOSONDE LAUNCH HEIGHT = 0.0 METRES

LEVEL	PRESS (mB)	TEMP (C)	RH (%)	DEW PT DEP(C)	METRES	N UNITS	N/Kft	M UNITS	CONDITION
1	1,026.2	18.8	73.8	4.7	0.0	343.0	-43.6	343.0	SUPER
2	1,014.5	17.4	65.9	6.4	98.4	328.9	-9.8	344.3	NORMAL
3	990.5	15.6	70.7	5.2	302.5	322.3	-2.1	369.8	NORMAL
4	969.0	13.8	82.4	2.9	488.4	321.0	-7.9	397.7	NORMAL
5	931.3	10.9	96.1	0.6	822.0	312.4	-13.1	441.4	NORMAL
6	836.7	4.9	97.5	0.4	1,707.8	274.2	-107.7	542.3	TRAP
7	825.2	5.2	10.1	30.0	1,820.8	234.3	-10.9	520.1	NORMAL
8	817.2	6.1	9.8	30.0	1,900.4	231.5	-10.8	529.8	NORMAL
9	810.1	6.3	8.8	30.0	1,971.9	228.9	-8.2	538.4	NORMAL
10	735.3	7.1	8.4	30.0	2,766.3	207.6	-6.1	641.8	NORMAL
11	695.7	3.6	9.1	30.0	3,218.1	198.5	-5.6	703.7	NORMAL
12	683.0	2.7	10.2	30.0	3,367.3	195.8	-6.4	724.3	NORMAL
13	637.1	0.1	10.2	30.0	3,927.0	184.0	-5.3	800.4	NORMAL
14	628.5	0.0	11.8	30.0	4,035.8	182.1	-5.4	815.6	NORMAL
15	620.0	-.7	12.5	30.0	4,144.6	180.2	-5.3	830.7	NORMAL
16	501.9	-12.6	14.5	30.0	5,794.8	151.3	------	1,060.9	------

SURFACE REFRACTIVITY: 343 --SET SPS-48 TO 344

Fig. 3.1 IREPS environmental data list for R/V Endeavor launch number 1.

The propagation conditions summary, reproduced in Fig. 3.2, is an EM system independent visual display and plain-language narrative assessment of expected refractive conditions. Vertical profiles of refractivity N as well as modified refractivity M are accompanied by a diagram showing the presence and vertical extent of any

existing ducts. Evaporation duct height and surface wind speed information is given along with brief statements concerning anticipated performance of surface-to-surface, surface-to-air and air-to-air EM systems.

Propagating radar waves experience constructive and destructive interference as direct path rays coincide with rays reflected from the earth's surface. The resultant amplitude of the radar wave is a function of the phase differences among the intersecting waves. As a result, radar lobes (constructive interference) are created with shadow zones (destructive interference) appearing in between (Halliday and Resnick, 1981). Knowledge of where these lobes and shadow zones occur can become an immediate tactical advantage in both offensive and defensive operations. IREPS version 2.2 produces radar coverage diagrams which displays the positions of the lobes and the shadow zones for any specified radar system and target at any desired probability of detection (POD).

Fig. 3.3 is an example of the IREPS radar coverage display product which also can be very useful in determining an EM systems maximum range capability. It depicts a specified EM system's area of coverage on a curved-earth, range-versus-height plot. Varying PODs are indicated by variations in the shading of the lobes. A numeric listing of some of the parameters used to generate the display, along with the location and time/date information of the profile, are included at the bottom of this product.

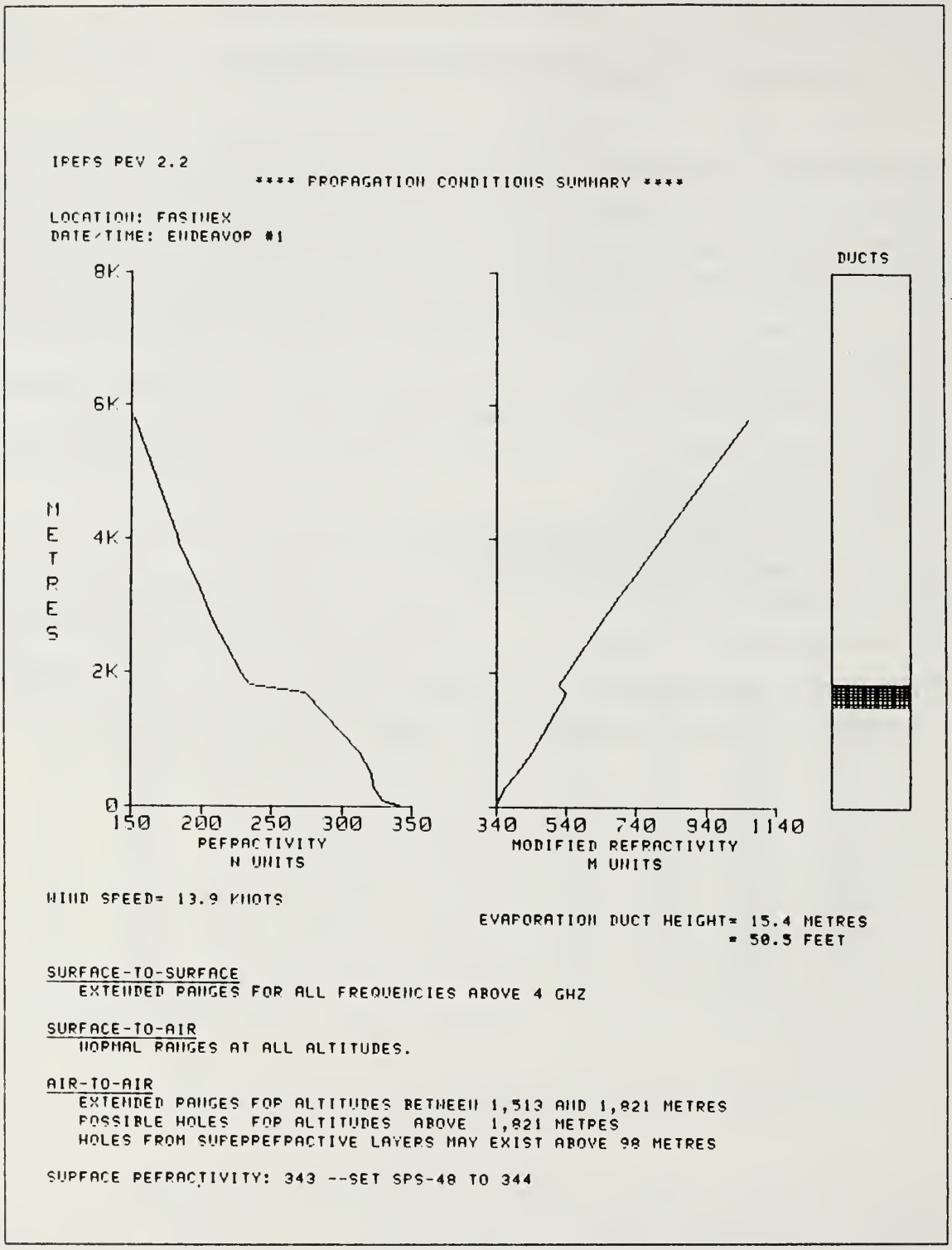

Fig. 3.2 IREPS propagation conditions summary for R/V Endeavor launch number 1.

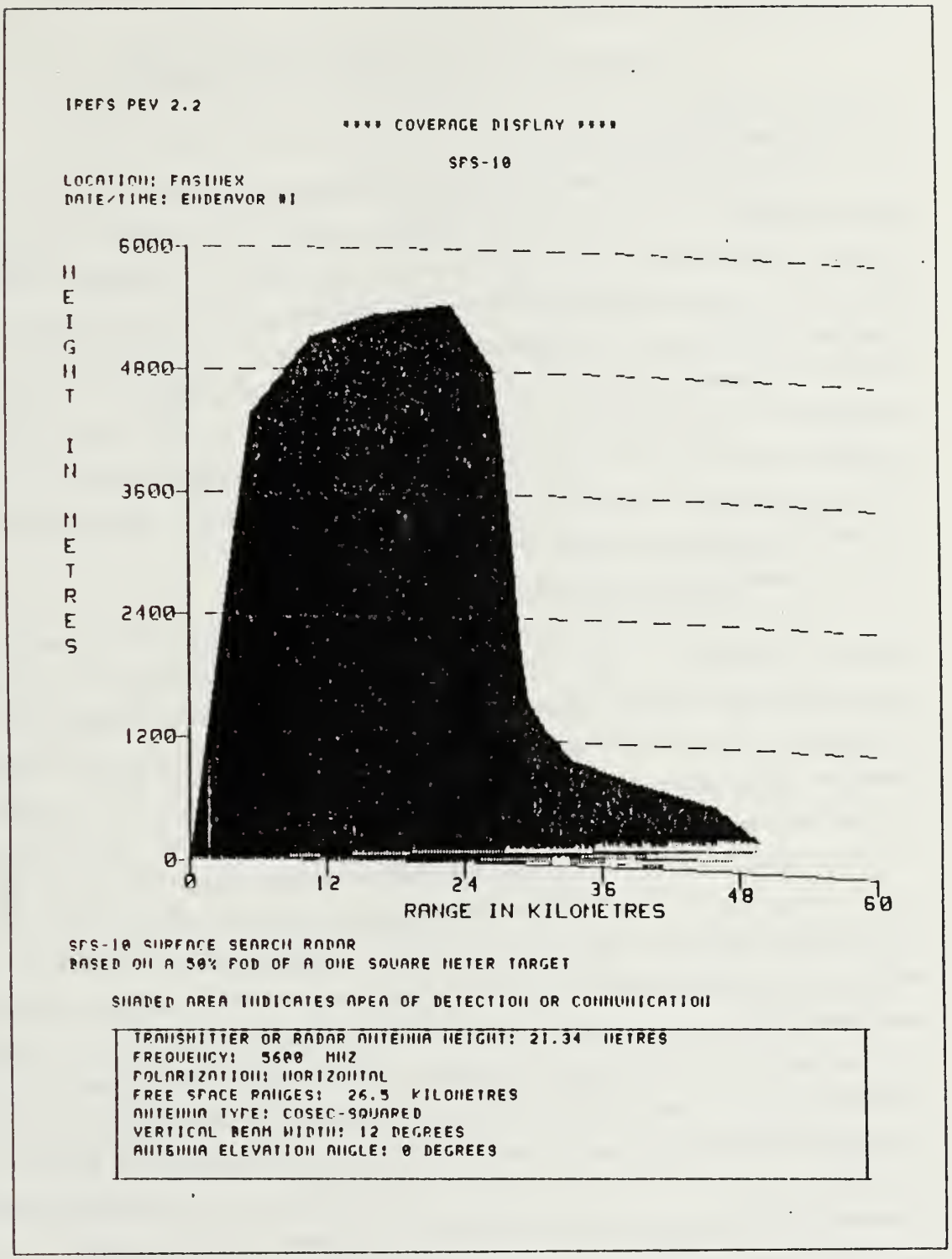

Fig. 3.3 IREPS radar coverage diagram for R/V Endeavor launch number 1.

IV. DATA SETS AND DATA PROCESSING

A. DATA SET SELECTION

Two separate data sets were used for this thesis study. Both sets of radiosondes provided high resolution data. The CAPTEX data provided atmospheric information every 20 m throughout the profile, whereas the FASINEX atmospheric data were separated by as much as 70 m at the surface, decreasing to 50 m near 500mb. A data set from a single station over land was chosen because the resulting analysis could be used to illustrate the evolution of atmospheric refraction conditions. The variability over land was expected to be very large in contrast to that over the ocean. The oceanic data were chosen to examine the notion that the MABL could be assumed to be homogeneous. Two ships in varying locations and separation distances were used to analyze the spatial variabilty of the MABL.

1. Cross Appalachian Tracer Experiment (CAPTEX)

The high resolution overland balloon soundings used for this study were recorded as a part of the CAPTEX research program. It was conducted in response to the increased concern over regional and international aspects of air pollution and the recognized need for more reliable long range predictions of atmospheric pollutant transport and dispersion. The CAPTEX field program was designed to "provide data to test, evaluate and improve the transport modules of long range pollution models. CAPTEX should also provide insight into dispersion mechanisms, the role of vertical shear, mixing processes in and above the planetary boundary layer, the adequacy of standard meteorological observations for determining dispersion, and the role of the Appalachians and the Great Lakes in modifying synoptic and subsynoptic atmospheric processes" (Ferber and Heffter, 1983). An extensive observation matrix, including supplementary (to the National Weather Service) rawinsonde launch sites and additional (up to four) launches each day, was designed to provide the data base necessary for forecasting and following the paths of released gaseous tracers. The CAPTEX data used in this thesis study were recorded at the Pennsylvania State University (PSU), which was one of the designated special rawinsonde sites. PSU was set up to launch up to four soundings per day beginning on the tracer release days and for several days afterward. The special soundings were scheduled for 0200L, 0800L,

1400L and 2000L (EDT). On the "non-experiment" days, two soundings per day were made. The data set begins on 0829L, 12 September 1983 (J.D. 255) and continues through 0130L, 30 October 1983 (J.D. 302).

Prior analysis of these data for purposes not related to air pollution (Vaucher, 1986) has clearly illustrated the significant variability in the atmospheric structure. Figs. 4.1, 4.2, and 4.3 show the time-height series of pressure altitude, temperature and water vapor pressure, respectively. Marked variations in the temperature and especially the water vapor pressure as a function of time and height produced significant variations in the atmospheric refractivity, N, structure. Fig. 4.4 shows both optical and microwave mean refractivity (N units) profiles. The magnitudes decrease approximately exponentially with height, corresponding to what would be expected climatologically (Bean and Dutton, 1966). Fig. 4.5 illustrates the variability of refractivity as a function of altitude: the standard deviation of N as a function of height was plotted. Water vapor pressure is the dominant variable forcing the fluctuations of the microwave refractivity which are nearly 2.5 fold greater than those for optical refractivity. The relative maxima in standard deviation near the surface and at 2000 meters height are most likely due to changes in the height of the inversion layer and in the atmospheric refractivity in response to diurnal variations in radiative heating, nocturnal cooling, and the larger scale synoptic variability occurring during the period of the experiment. The relative minimum between the two can be related to the characteristic of the mixed layer which tends to keep conditions well-mixed resulting in smaller fluctations from the mean value of N than can be seen in either the surface layer below or the inversion layer above.

2. **Frontal Air-Sea Interaction Experiment (FASINEX)**

Previous air-sea interaction experiments, including JASIN (Pollard, 1978), have done little to determine what role horizontal variability might play in air-sea interaction. "However, the JASIN results were sufficient to point out the shortcomings of air-sea-interaction experiments that concentrate on observing the evolution and modification of boundary layer structure in only the vertical and to stimulate plans for experiments like FASINEX in which attention is focused on horizontal as vertical variability" (Stage and Weller, 1985).

FASINEX was a "study of the response of the upper ocean to atmospheric forcing in the vicinity of an oceanic front, the response of the lower atmosphere in that vicinity to the oceanic front, and the two-way interaction between the ocean and the

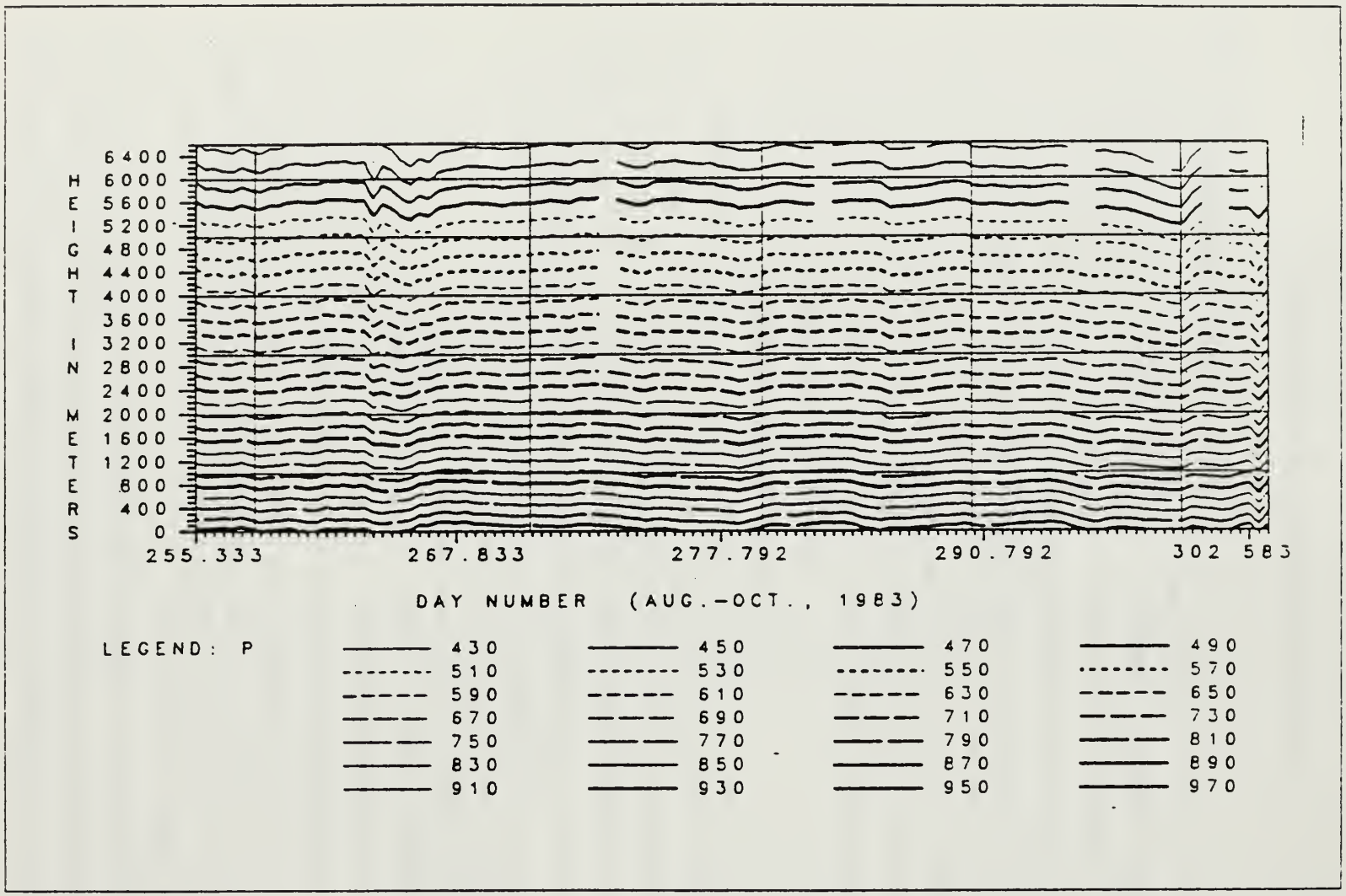

Fig. 4.1 Time height fluctuations of pressure altitude from Vaucher (1986).

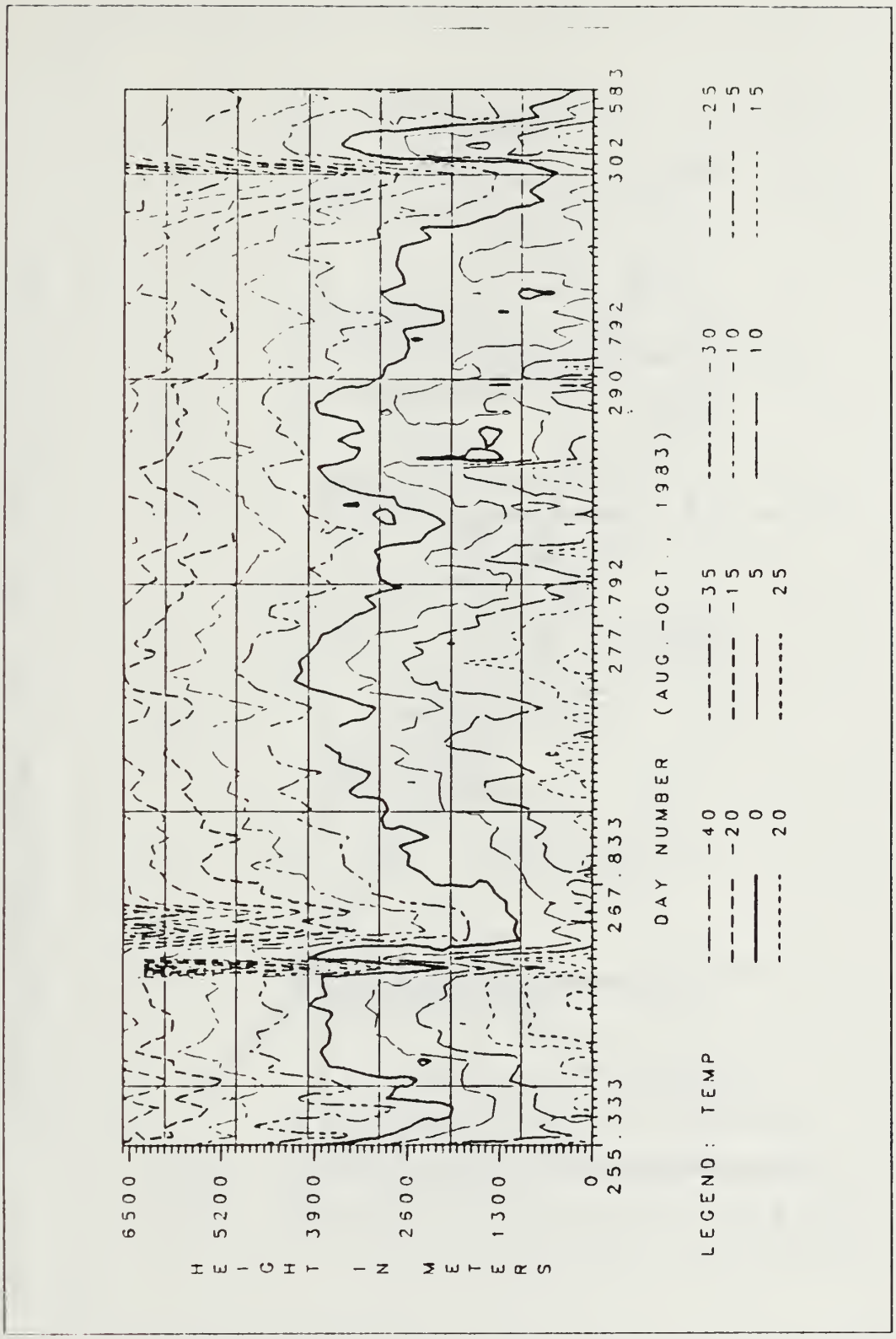

Fig. 4.2 Time height fluctuations of temperature from Vaucher (1986).

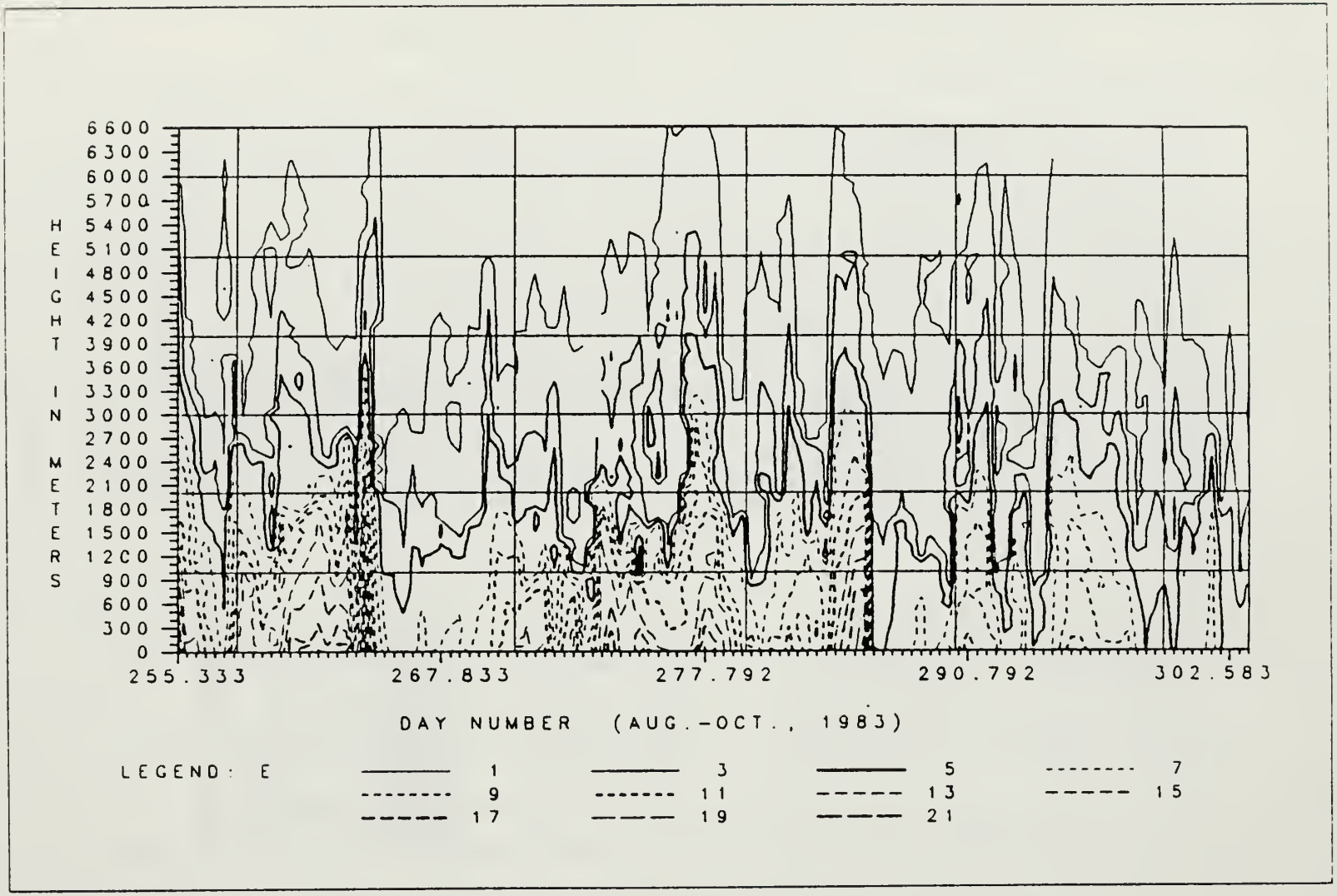

Fig. 4.3 Time height fluctuations of water vapor pressure from Vaucher (1986).

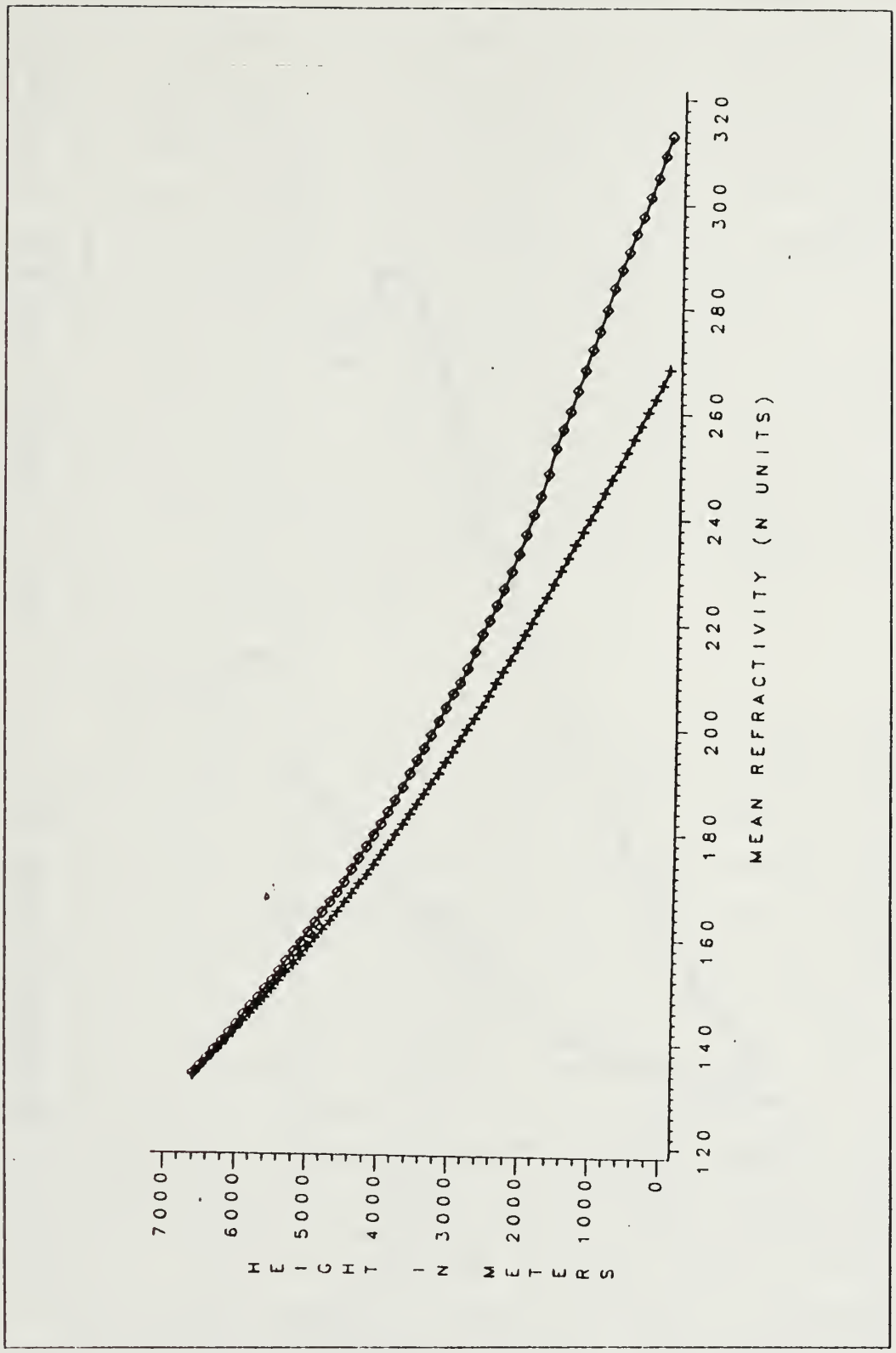

Fig. 4.4 Mean optical and microwave refractivity, N, as a function of height from Vaucher (1986).

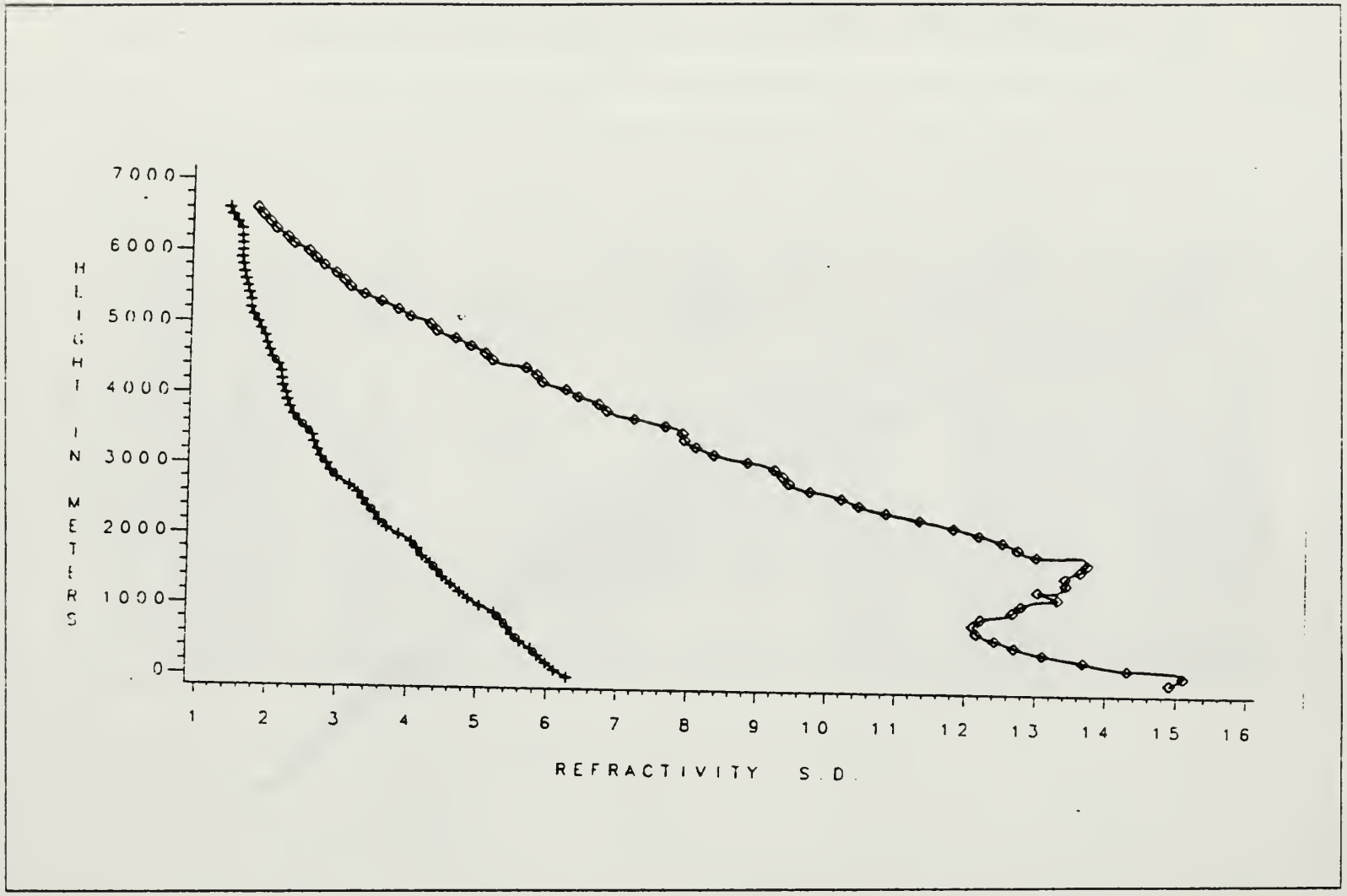

Fig. 4.5 Standard deviation of optical and microwave refractivity as a function of height from Vaucher (1986).

atmosphere in the subtropical convergence zone southwest of Bermuda" (Stage and Weller, 1986). Although the entire experiment was conducted from the winter of 1985 through the summer of 1986, the data used in this thesis study were obtained from radiosonde launches made by two oceanographic research vessels. The R/V Oceanus and the R/V Endeavor made extensive meteorological observations throughout phase 2 of the experiment during February and March 1986. The information gathered on board these two ships was used to investigate the horizontal homogeneity of the atmosphere. The objective was to compare the differences in the atmosphere over each vessel while they remained, at times, on opposite sides of an oceanic front.

In order to minimize contamination of the data set caused by temporal variations in the atmosphere, only radiosonde launches that were made at similar times by each ship were compared. Of the 132 launches made by both ships, 13 pairs of radiosonde launches were within 37 minutes or less of each other. Table 1 gives the positions of each ship during the 13 pairs of launches, their separation distances, and the difference in radiosonde launch times. Figs. 4.6 and 4.7 display the position of each ship at the time of each launch.

B. DATA PROCESSING

1. CAPTEX Data

Fig. 4.8 is a flow digram of the CAPTEX data processing steps. The CAPTEX data were obtained from PSU (Thomson, 1986). In order to compare the differences in IREPS products on atmospheric soundings of differing resolution, the 120 high resolution CAPTEX soundings were first degraded to resemble standard U.S. Navy operational soundings by selecting every fourth data point. This criterion is based on information from the Federal Meteorlogical Handbook No. 3, Radiosonde Observations (FMH #3). These two sets of CAPTEX data were then analyzed separately to avoid prejudice in significant and mandatory level selection. After plotting the 120 temperature and dew-point temperature profiles of the degraded CAPTEX soundings on a standard skew T-log P chart, they were given to a qualified Aerographers Mate along with a copy of the pertinent pages of the Federal Meteorological Handbook No. 4, Radiosonde Code (FMH #4). AG2 Marty Schy then determined the significant and mandatory levels for each degraded sounding using the guidance in FMH #4. The temperature and dew-point profiles of the 120 high resolution CAPTEX soundings were plotted with the aid of GRAFSTAT, an interactive plotting routine avaliable on the IBM 3033 mainframe at the Naval

TABLE 1

POSITIONAL INFORMATION FOR BOTH SHIPS AT THE TIMES OF EACH LAUNCH

LAUNCH NUMBER	SHIP POSITIONS R/V OCEANUS	R/V ENDEAVOR	SEPARATION (KM)	DELTA TIME (MIN)
1	27.4N 69.6W	28.2N 70.5W	125.6	0
2	28.1N 70.3W	28.5N 70.5W	50.0	26
3	28.8N 70.6W	28.8N 70.2W	37.6	15
4	28.2N 70.1W	28.9N 70.0W	69.9	26
5	29.0N 69.9W	28.2N 70.1W	87.7	37
6	28.2N 69.7W	27.9N 69.8W	36.6	15
7	28.7N 70.1W	27.2N 69.8W	172.7	19
8	28.2N 68.4W	28.4N 68.4W	21.3	1
9	28.6N 68.1W	28.5N 68.1W	9.0	26
10	28.8N 68.1W	28.9N 67.9W	23.7	34
11	27.3N 69.3W	28.8N 67.6W	237.9	35
12	27.1N 69.6W	28.6N 67.3W	276.8	3
13	26.9N 70.0W	28.8N 67.5W	333.4	15

Postgraduate School. Significant and mandatory levels were determined by the author using the guidance of FMH #4. Pressure, temperature and dew-point temperature information for all significant and mandatory levels from both CAPTEX data sets were input into the IREPS version 2.2 refractivity code. Output information included, dM/dz values between the levels; ducting occurrences; and duct level, thickness and strength information. Statistical analysis of these numeric values included average duct strength, average duct thickness, and standard deviation of the duct thickness for both the high resolution and degraded resolution profiles. The results of the statistical analysis of IREPS output appear in the results section, Chapter five, of this thesis.

2. **FASINEX Data**

Fig. 4.9 is a flow diagram of the steps involved in the FASINEX data processing. After choosing the 13 pairs of soundings within 37 minutes or less of each

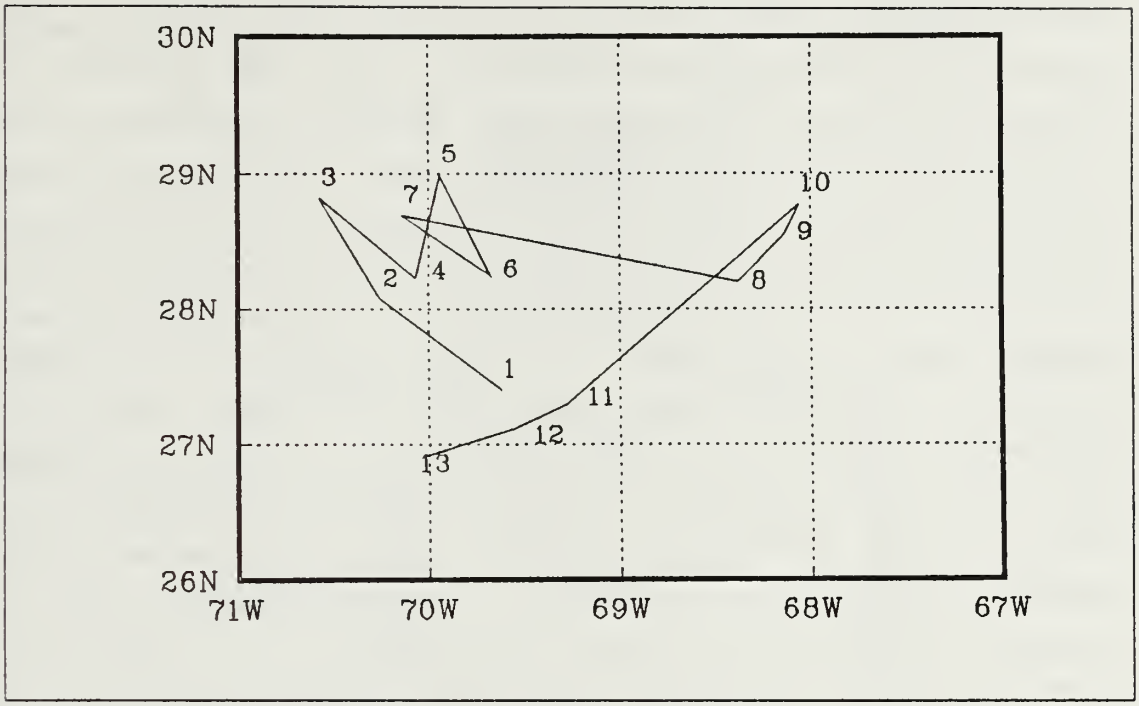

Fig. 4.6 R/V Oceanus radiosonde launch positions.

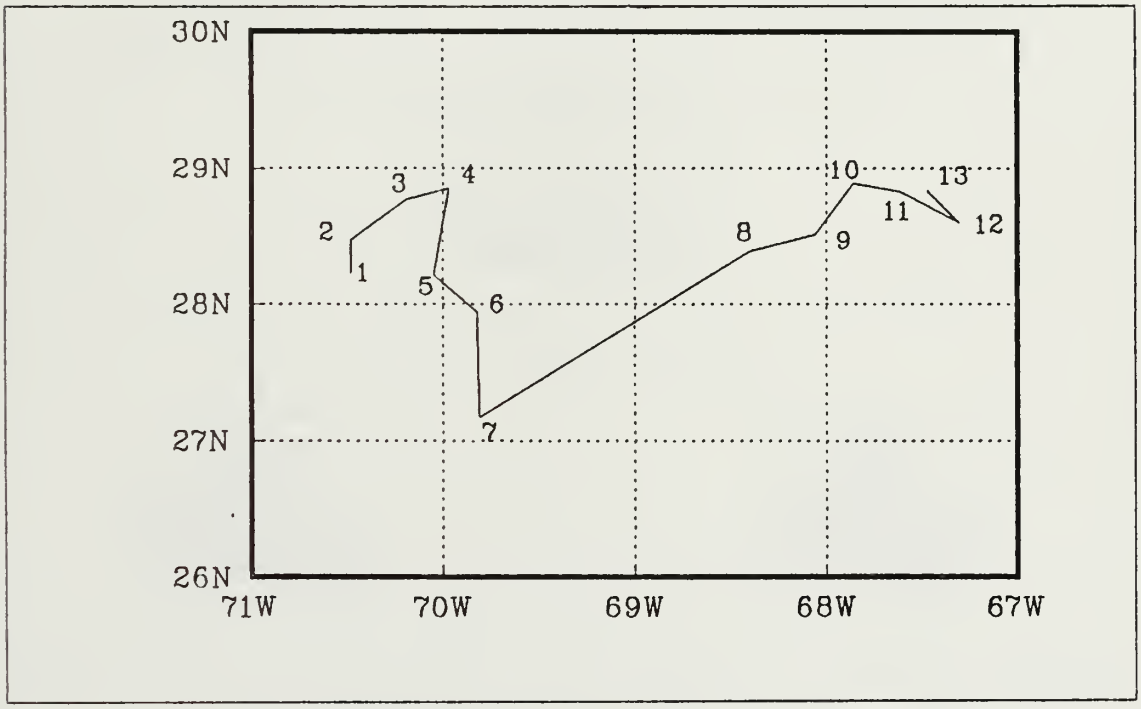

Fig. 4.7 R/V Endeavor radiosonde launch positions.

other, the height of the sounding reaching the greater altitude was truncated so that each sounding pair would extend to the same altitude. These 26 launches were then prepared for the IREPS code by plotting, once again using GRAFSTAT, the temperature and dew point temperature profiles. Significant and mandatory levels were determined using the guidance in FMH #4. Pressure, temperature, and dew-point temperature information from each selected level, along with sea-surface temperature and surface wind speed information, was then entered into the IREPS code to produce the refractive structure of the atmosphere over each ship. Ship separation distance was computed using a simple great circle distance algorithm. Other statistical manipulations were similar to those applied to the CAPTEX data. Additionally, the information was entered into a modified IREPS version 2.2 radar coverage diagram code to obtain radar propagation and coverage information. This modification did not change any of the mathematical manipulations used to derive the radar coverage diagrams; it merely involved the addition of programing statements which could determine the farthest extent of a lobe. For the purposes of this thesis study, the extent of a radar lobe was defined to be the maximum range and corresponding height reached by that lobe. With these two quantitative measurements of lobe characteristics, meaningful statistics and comparisons between lobes could be achieved.

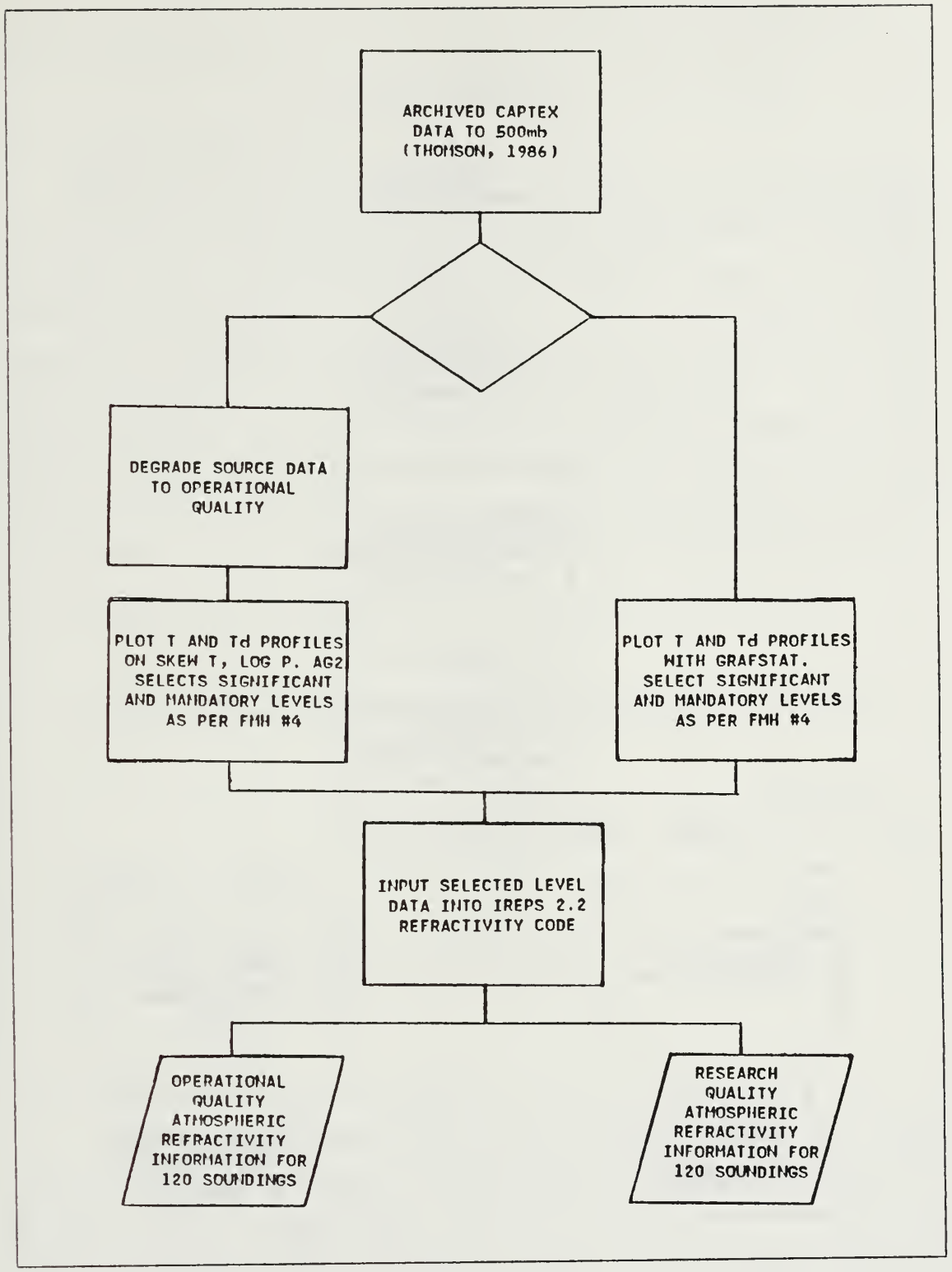

Fig. 4.8 Flow diagram of CAPTEX data processing steps.

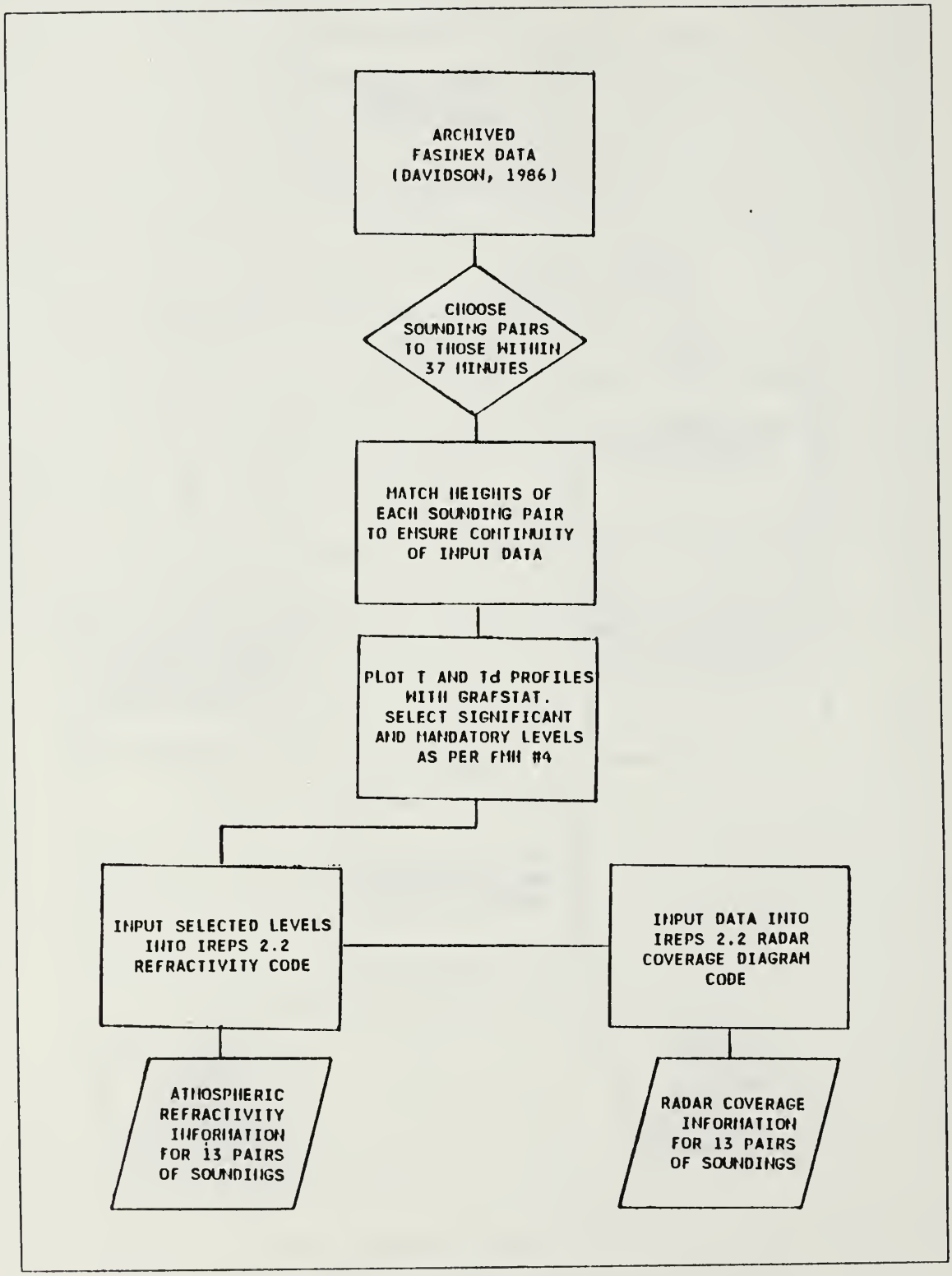

Fig. 4.9 Flow diagram of the FASINEX data processing steps.

V. RESULTS

A. CAPTEX RESULTS

The results of comparing the high resolution radiosonde data with the degraded data are shown in Table 2. As one might expect, the high resolution data produced a far more detailed refractive structure, revealing almost five times as many ducts. Because the high resolution data produced thin ducts in the profiles which were smeared out in the degraded data, the average thickness of the predicted ducts using the low resolution data was 31.8% larger than the average thickness of those from the high resolution data base. The standard deviation of the duct thickness was slightly larger as was the average duct strength for the high resolution soundings. This is due to the ability of the high resolution data to more accurately define the top and bottom of the ducts and to observe the greater M value differences between those heights.

TABLE 2
STATISTICAL RESULTS OF HIGH VS. DEGRADED RESOLUTION DATA

	HIGH RESOLUTION DATA	DEGRADED RESOLUTION DATA
NUMBER OF DUCTS	68	14
AVG. THICKNESS (M)	115.95	152.79
σ DUCT THICKNESS (M)	57.58	50.87
AVG. DUCT STRENGTH (M UNITS)	4.53	4.27

Another interesting result of comparing the degraded and the high resolution ducting layer results was that the high resolution sounding enabled resolution of multiple ducts in a single sounding. In some cases, the degraded sounding merely merged two slightly separated ducts into a single duct. This result is particularly important when considering that the minimum frequency that can be trapped by a duct

is a direct function of the thickness of the duct (Kerr, 1951). In most cases where a secondary duct was relatively shallow, the degraded resolution soundings missed the duct altogether. Fig. 5.1 is a matrix of the number of ducts produced by the high resolution soundings compared to the number of ducts produced by the degraded resolution soundings for each launch. The strong bias toward the lower side of the diagonal is a direct indication of a high resolution sounding's ability to better delineate the smaller scale refractive structure.

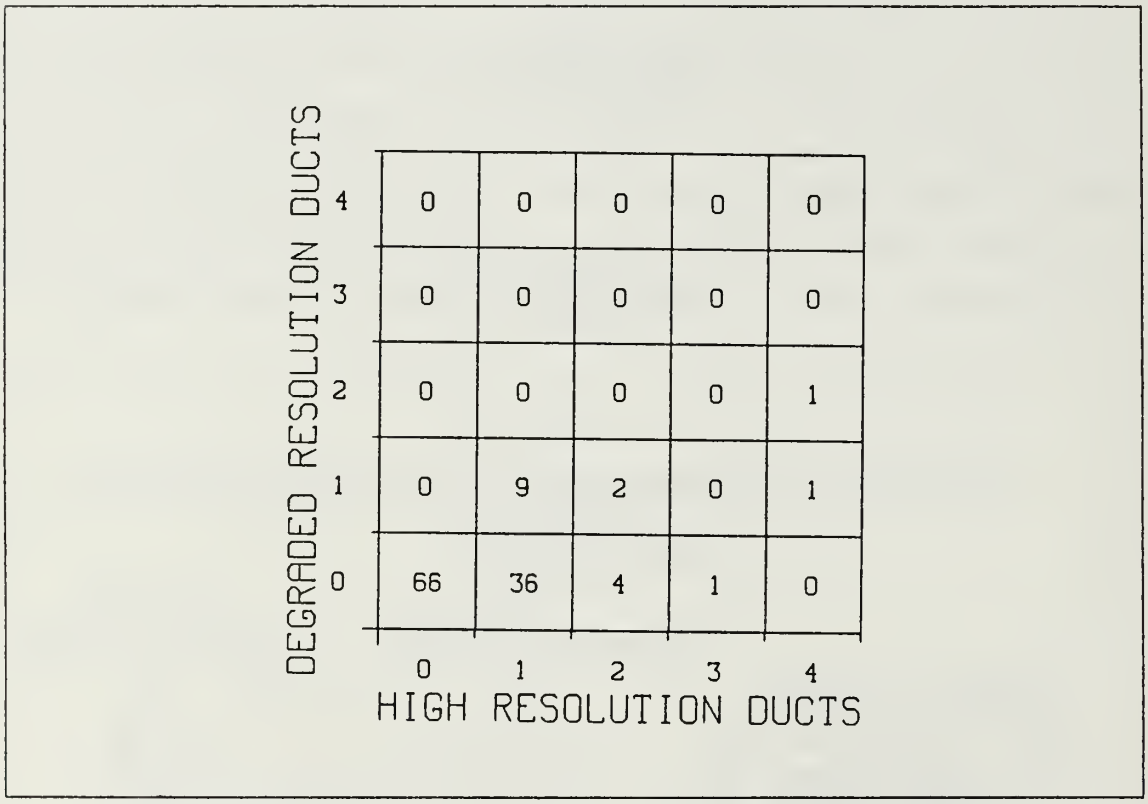

Fig. 5.1 Number of ducts discovered by each data set.

Figs. 5.2 and 5.3 are histograms of duct heights for both the high resolution and degraded resolution CAPTEX data, respectively. This representation of the CAPTEX results once again shows that high resolution input data are required to observe the fine refractive structure of the atmosphere. Figs. 5.4 and 5.5 are a surface plot representation of duct evolution over time for both the high and low resolution data, respectively. Only the high resolution data are capable of realistically representing the ambient ducting conditions.

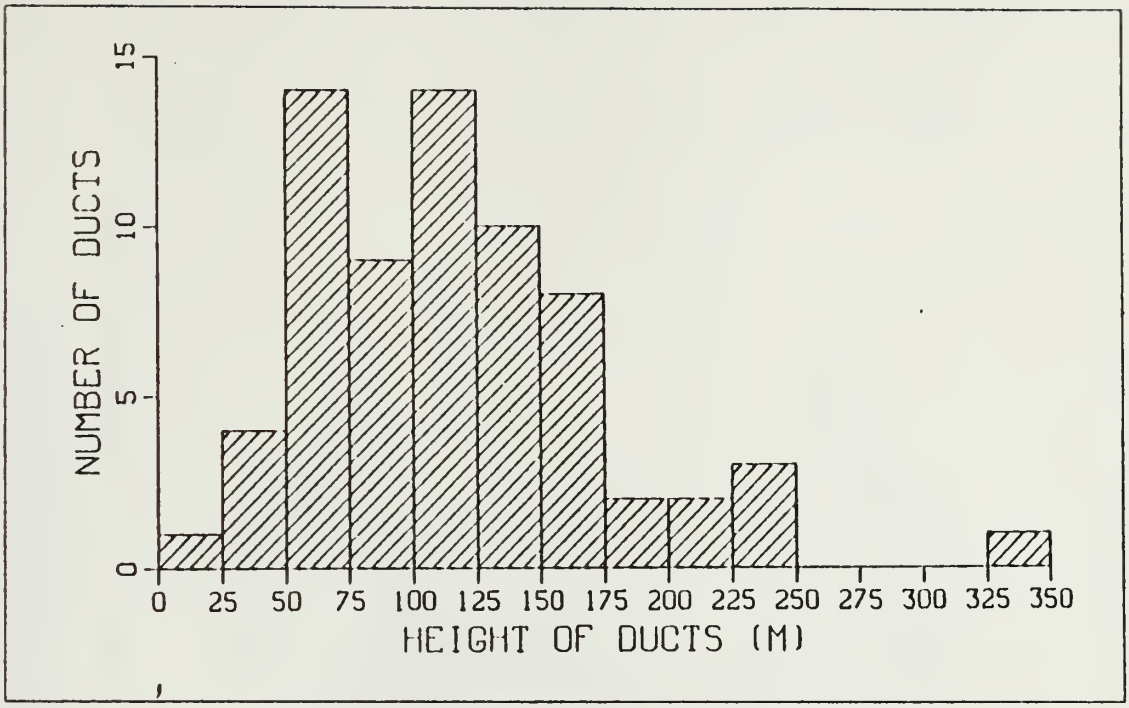

Fig. 5.2 Histogram of CAPTEX high resolution data duct heights.

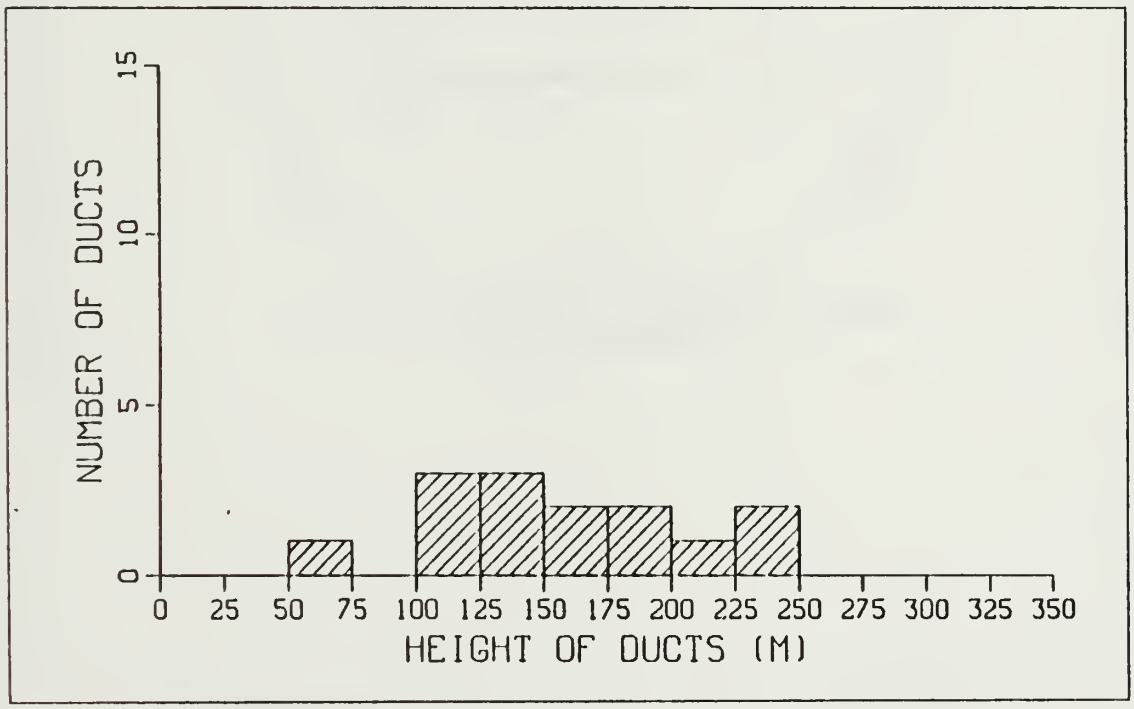

Fig. 5.3 Histogram of CAPTEX low resolution data duct heights.

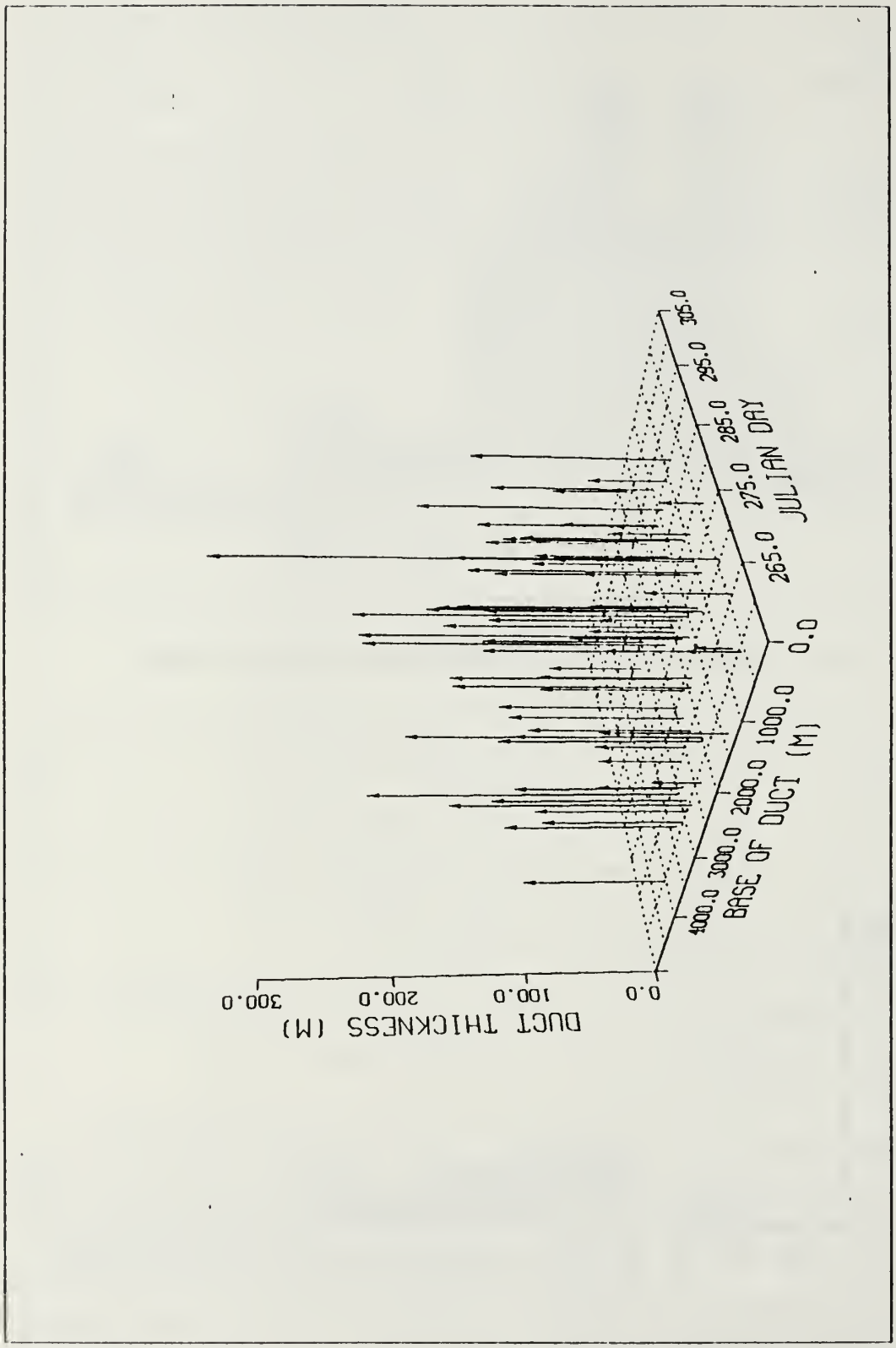

Fig. 5.4 Surface plot of duct evolution for the high resolution data.

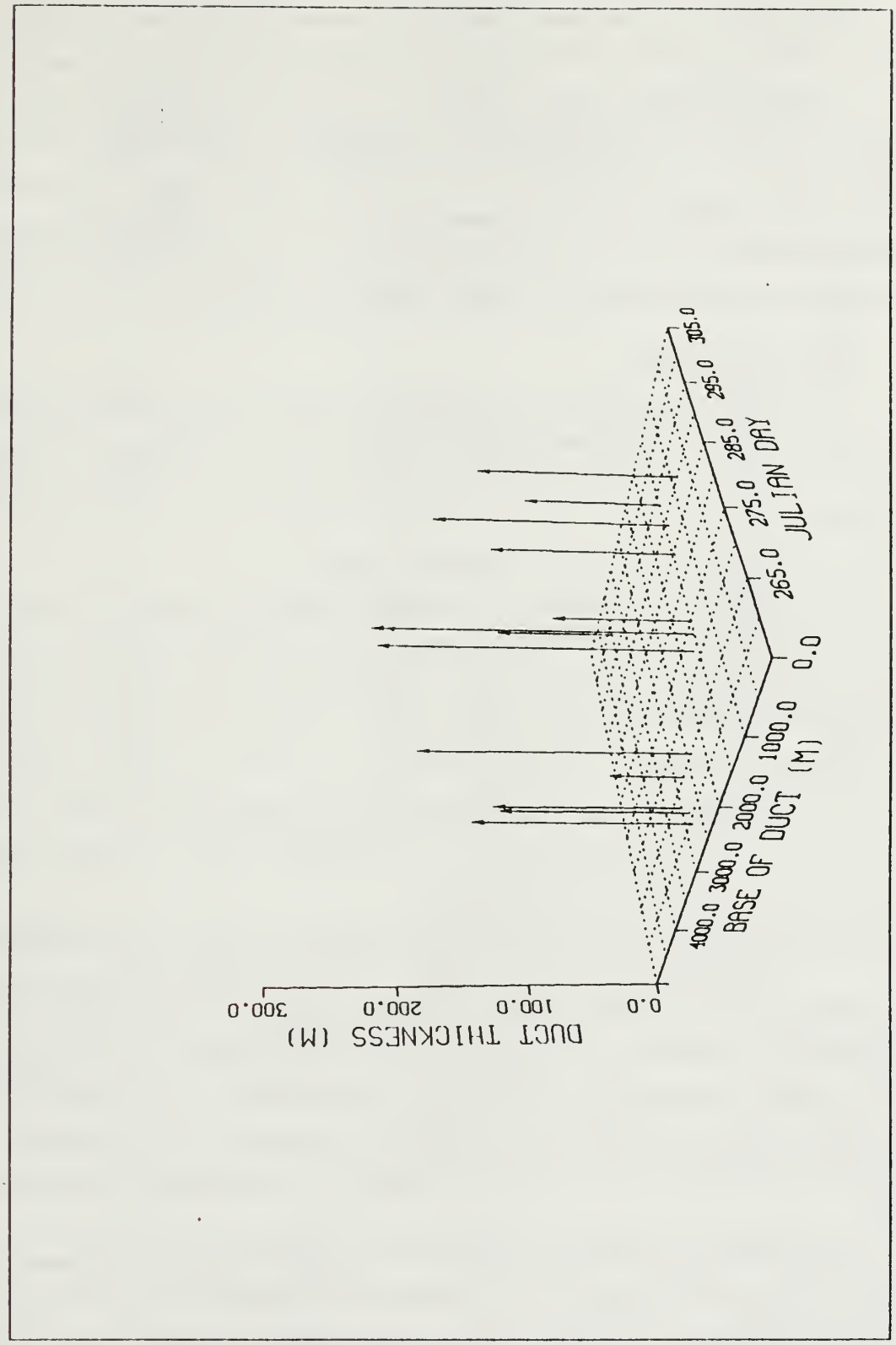

Fig. 5.5 Surface plot of duct evolution for the low resolution data.

Visual inspection of the time variability of ducting features depicted in Fig. 5.4 gives an indirect indication of how quickly the refractive environment can change. Not only are ducting features varying in height and extent over relatively short time periods, but they are also appearing and dissappearing. While MABL refractive variability may not be as dramatic as this continental data, IREPS users need to consider the timeliness of the input data, with respect to changing environmental conditions, before assuming atmospheric refractive conditions outputs are valid products capable of representing the present state of the atmosphere.

B. FASINEX RESULTS

Table 3 denotes the sea-surface temperature recorded at each ship during the 13 pairs of launchings and, using an absolute difference in water temperature of at least one degree C, indicates whether the ships were on the same side or on opposite sides of an oceanic front.

Using this information, Fig. 5.6 and Table 4 were derived.

Distinct differences in MABL structure can be expected on opposite sides of an oceanic front (Stage and Weller, 1985). One would expect that the colder water side of the front should usually be associated with a more stable, less convective MABL and would thus allow higher evaporation ducts to exist. Conversely, the warmer water side should enhance convective activity resulting in turbulent motion supressing evaporation duct gradients. Fig. 5.6 shows a trend of the higher ducts existing on the colder side of the front supporting the above assumption; however, more data points are needed to precisely define this phenomenon.

In an effort to ascertain if elevated duct occurrence is related to warm side/cold side variations, Table 4 provides some insight. The cold side elevated ducts were 48.2% greater in mean strength and 51.2% greater in mean thickness than the warm side elevated ducts. Ducting occurences were 40% more prevalent on the cold side of the front. Again, since only six data points were used, the exact cause-effect relationships cannot be unambiguously determined; however, the results show a definite trend of larger, stronger and more frequent duct occurrences in colder water regimes.

Table 5 shows the variability in elevated duct occurrences and evaporation duct heights observed by each ship. Fig. 5.7 shows that the differences in the evaporation duct heights observed by each ship are not a simple function of distance. The results of this figure indicates that one cannot assume similar atmospheric refractive

TABLE 3

OBSERVED SEA SURFACE TEMPERATURES DURING THE FASINEX SHIP LAUNCHES

LAUNCH NUMBER	SEA-SURFACE TEMPERATURES (°C) R/V ENDEAVOR	R/V OCEANUS
1	21.0 (C)	23.5 (W)
2	21.3 (C)	23.4 (W)
3	21.9	21.1
4	21.9	22.4
5	23.0 (W)	21.7 (C)
6	23.3	23.0
7	23.3	22.6
8	23.1	22.9
9	22.8	22.5
10	21.8	22.6
11	22.0 (C)	23.5 (W)
12	21.4 (C)	24.2 (W)
13	22.5 (C)	24.1 (W)

(C) and (W) indicate cold and warm water areas respectively

conditions based merely on short separation distances; conversely, great separation distances do not always imply large variations in refractive conditions.

Using IREPS coverage diagrams, the variations in radar lobe heights and ranges between the pairs of launches were investigated. The most widely used radar in the U.S. Navy is the SPS-10 surface search radar found on board most surface combatants, amphibious ships and auxiliaries (Polmar, 1985). The SPS-10 radar parameters needed to generate the radar coverage diagrams are unclassified. Accordingly, it was the radar of choice for this trial. Comparing the differences in the maximum heights and ranges of the four radar lobes using a 50% POD on a one square meter fluctuating target, Figs. 5.8 through 5.15 again show differences in refractivity and radar propagation conditions of the atmosphere cannot be directly correlated simply with distance alone.

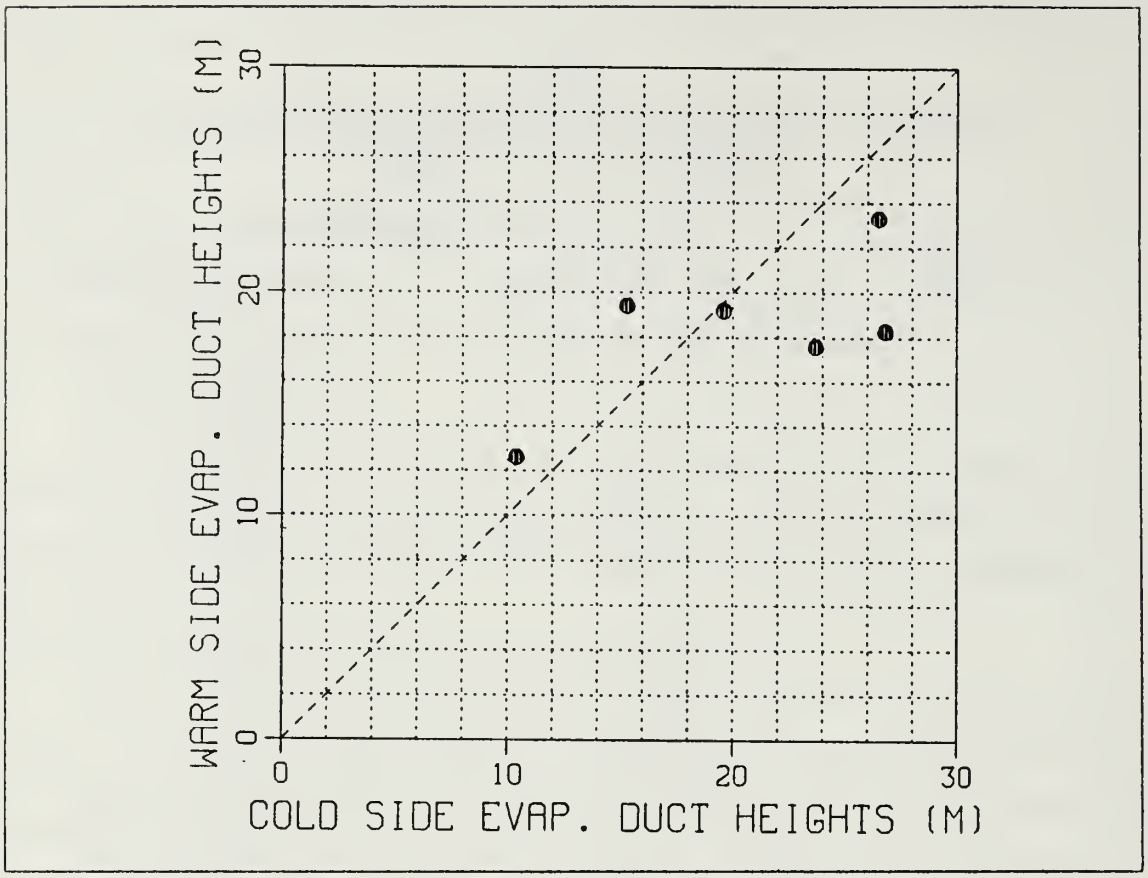

Fig. 5.6 Cold side versus warm side duct heights.

It is believed that only with knowledge of the synoptic-scale and mesoscale variability of the surrounding environment can meaningful interpretations of IREPS output be achieved. A real tactical disaster could result from blindly assuming homogeneous refractive conditions. Importantly, these results only depict refraction variations in a straight line path between two ships. Actual tactical situations involve 4-dimensional problems and the variations in atmospheric refractivity over the domain will be a function of the varying atmospheric conditions.

TABLE 4

ELEVATED DUCT SUMMARY FOR WARM/COLD SIDE OCCURRENCES WITH ELEVATION IN METERS AND STRENGTH IN M UNITS

LAUNCH NUMBER	ELEVATED DUCTS			
	WARM SIDE		COLD SIDE	
	ELEVATION	STRENGTH	ELEVATION	STRENGTH
1			1512.65-1820.52	22.24
2			640.61- 810.28	6.81
			1655.02-1714.35	2.46
5			2173.17-2243.29	0.16
11	1000.09-1123.74	6.15	1120.36-1444.83	16.34
	1261.05-1434.52	9.51		
12	1269.88-1381.17	6.53	1190.63-1590.62	31.38
13	637.77- 838.88	17.98	1006.46-1185.62	5.86
	2835.71-2939.90	0.95		
Number of Ducts =	5		= 7	
Average Thickness =	142.74		= 215.80	
Mean Strength =	8.22		= 12.18	

TABLE 5

ELEVATED DUCT OCCURRENCES AND EVAPORATION DUCT HEIGHTS AT BOTH SHIPS FOR EACH LAUNCH

LAUNCH NUMBER	ELEVATED DUCTS R/V ENDEAVOR	ELEVATED DUCTS R/V OCEANUS	EVAPORATION DUCT HEIGHT (M) R/V ENDEAVOR	EVAPORATION DUCT HEIGHT (M) R/V OCEANUS
1	1	0	15.3	19.4
2	2	0	21.3	19.2
3	0	0	7.6	11.4
4	0	0	9.8	23.2
5	2	1	17.6	23.7
6	1	0	40.0	21.7
7	1	1	22.2	20.3
8	0	2	6.6	9.3
9	1	1	16.6	21.6
10	0	1	18.1	17.0
11	1	2	10.4	12.6
12	1	1	26.5	23.3
13	1	2	26.8	18.3

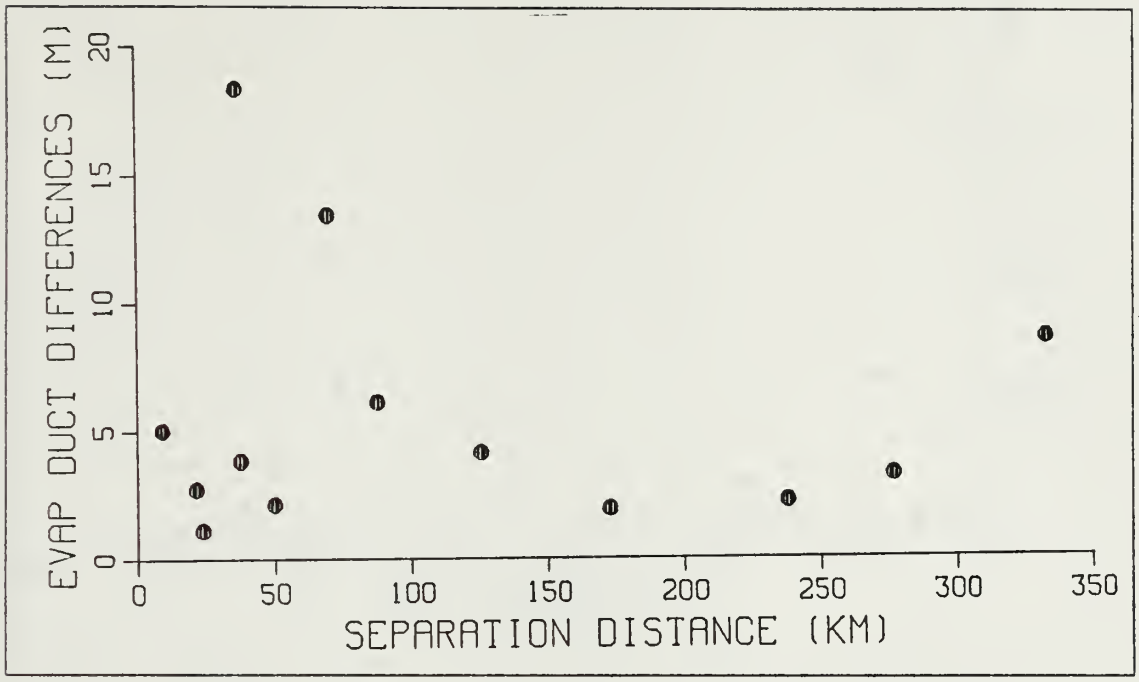

Fig. 5.7 Differences in evaporation duct height as a function of ship separation distance.

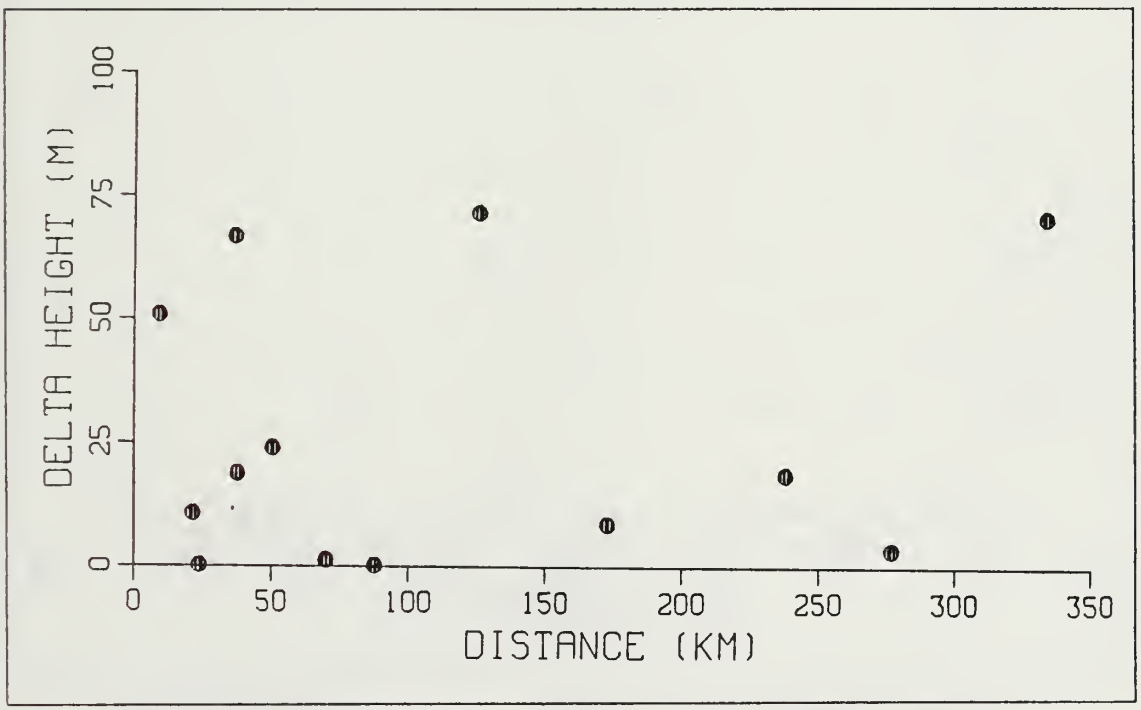

Fig. 5.8 Differences in 50% POD lobe 1 heights for a SPS-10 radar.

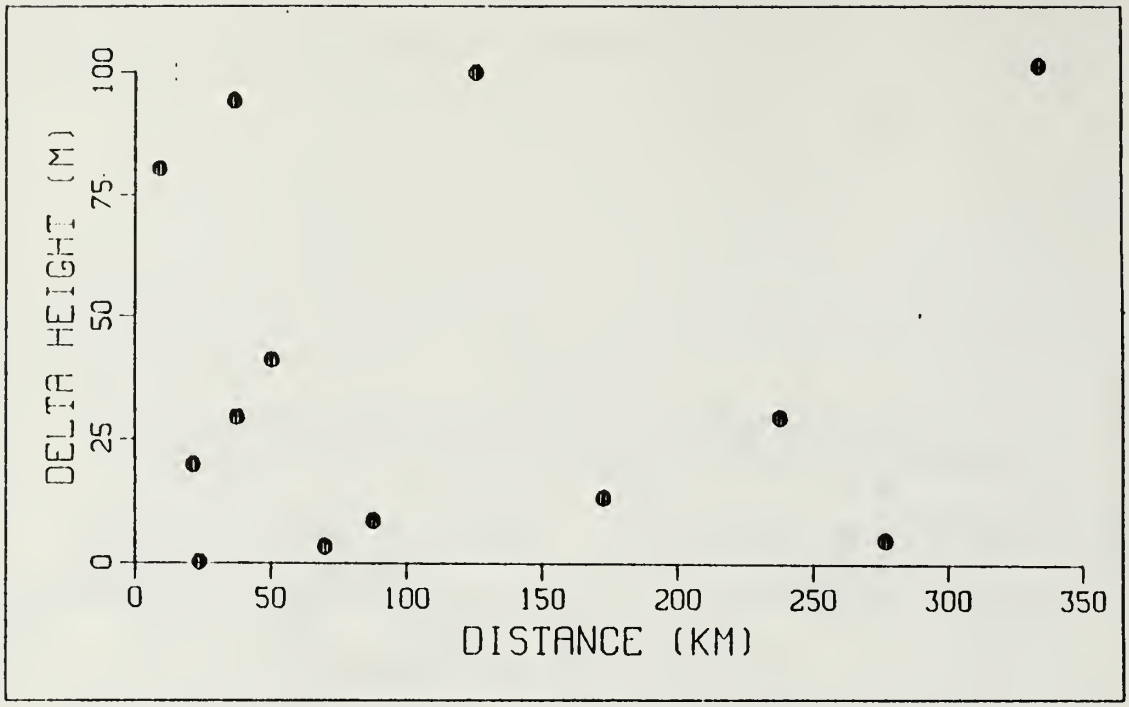

Fig. 5.9 Differences in 50% POD lobe 2 heights for a SPS-10 radar.

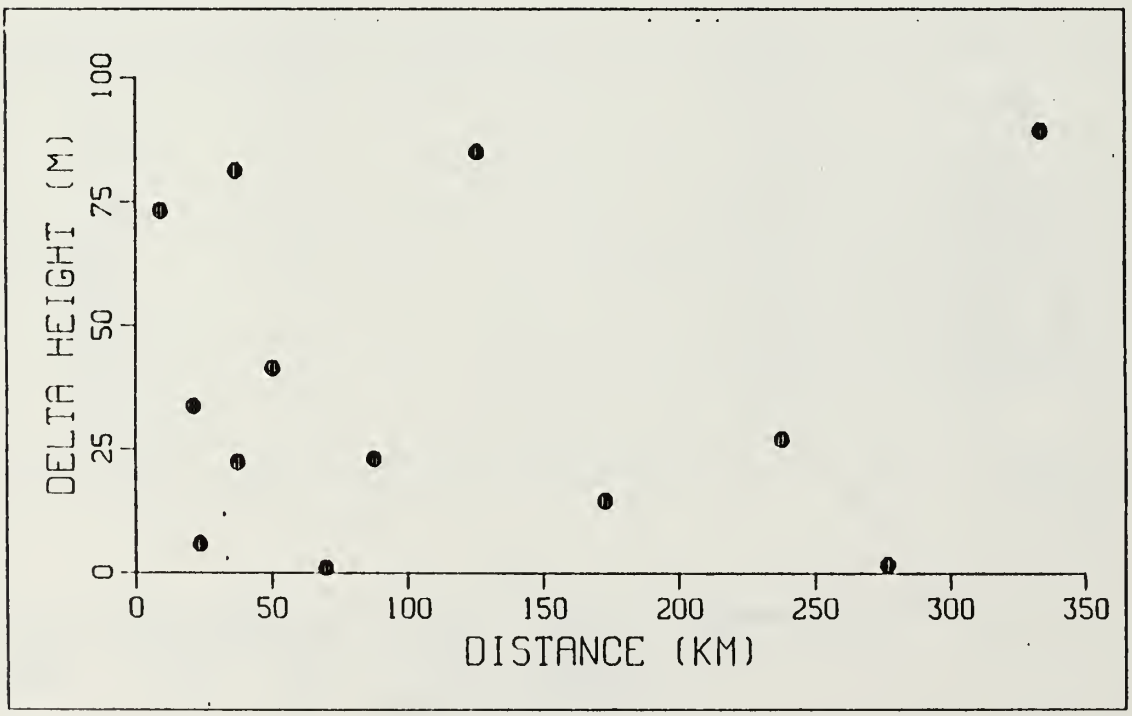

Fig. 5.10 Differences in 50% POD lobe 3 heights for a SPS-10 radar.

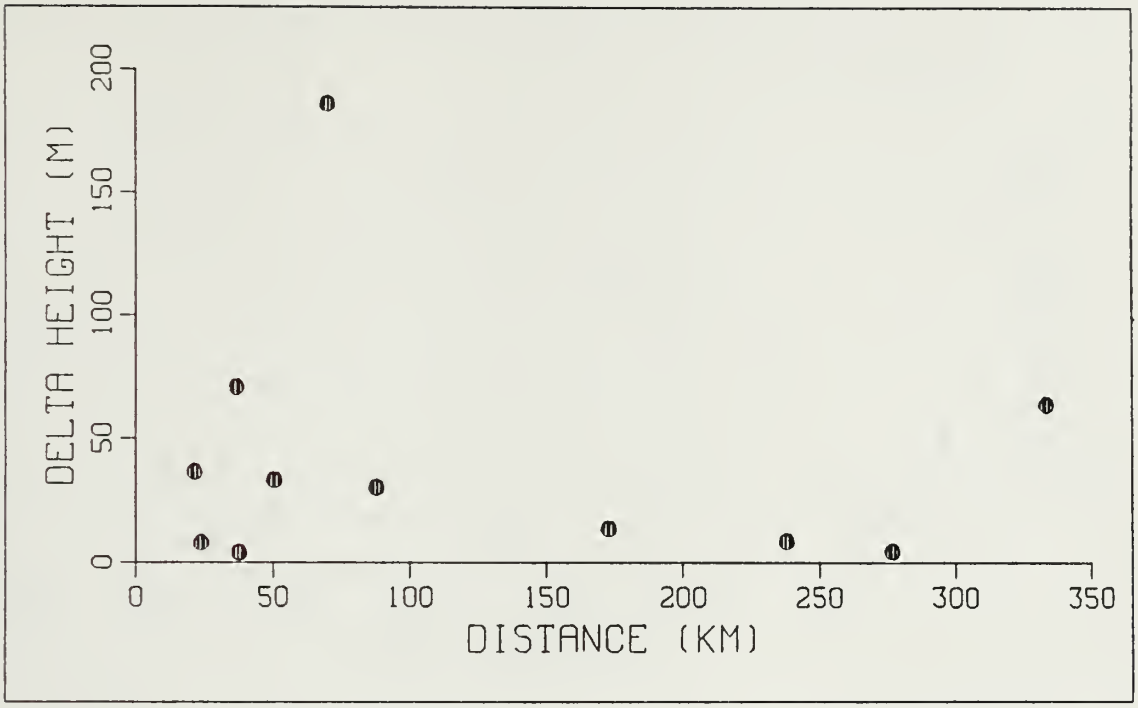

Fig. 5.11 Differences in 50% POD lobe 4 heights for a SPS-10 radar.

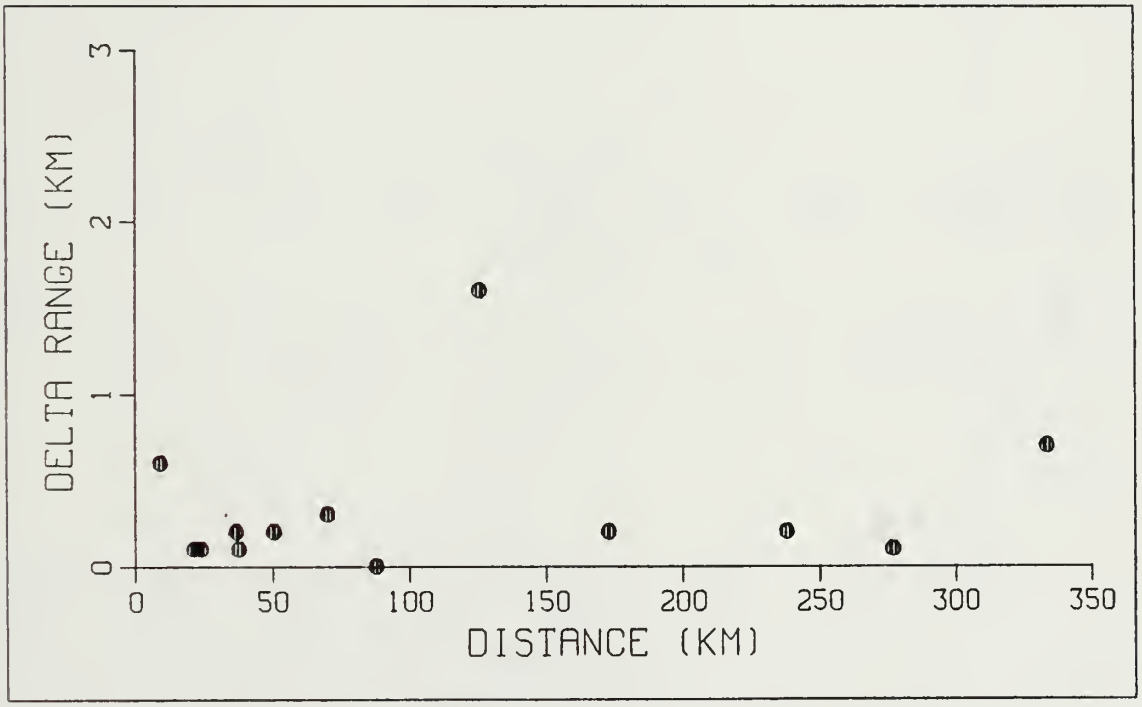

Fig. 5.12 Differences in 50% POD lobe 1 ranges for a SPS-10 radar.

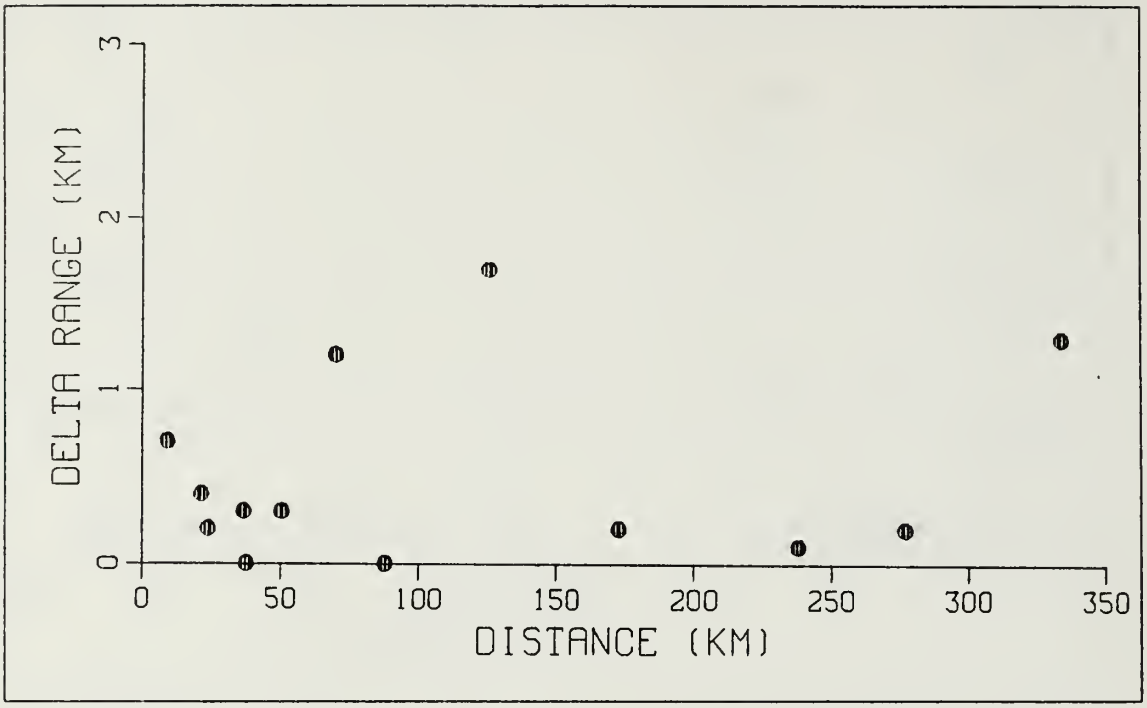

Fig. 5.13 Differences in 50% POD lobe 2 ranges for a SPS-10 radar.

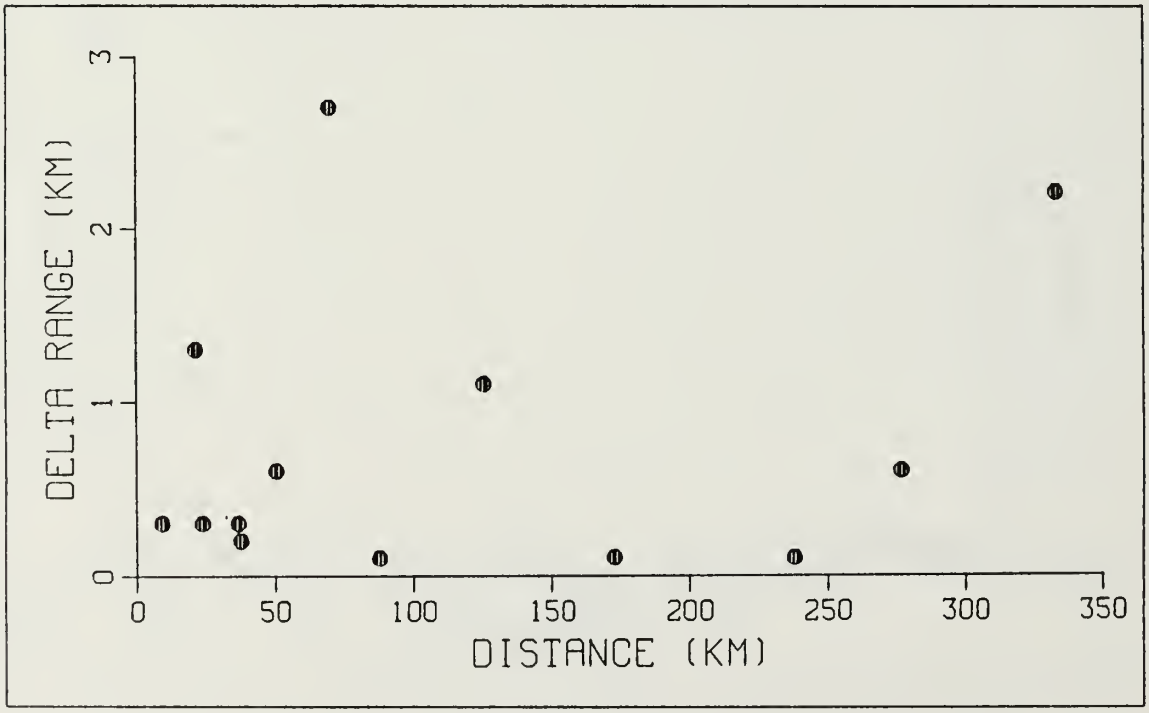

Fig. 5.14 Differences in 50% POD lobe 3 ranges for a SPS-10 radar.

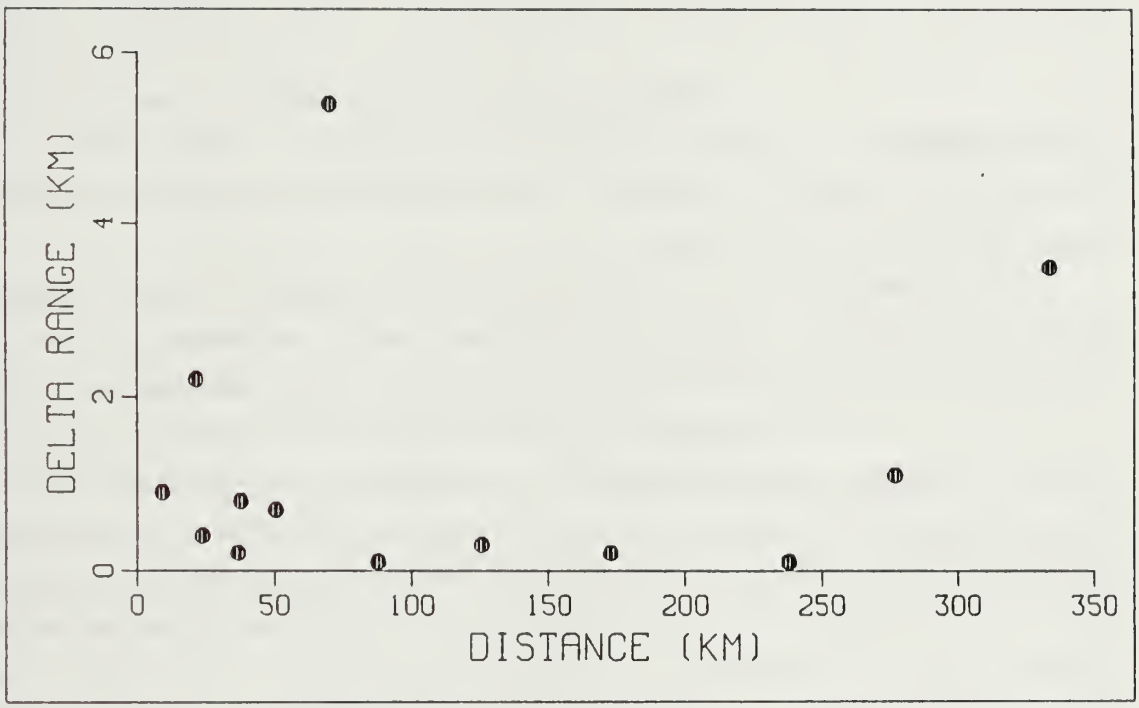

Fig. 5.15 Differences in 50% POD lobe 4 ranges for a SPS-10 radar.

VI. POSSIBLE VARIABILITY IN LOCAL REFRACTIVITY

A. SMALL SCALE REFRACTIVITY VARIABILITY

Spaced-cavity refractometers supported by a captive ballon provide the ability to examine the small scale, atmospheric layers of large variance in refractivity. Vertical variations of as much as 8 N units in as little as one meter were discovered using this technique (Lane, 1964). The steepest gradients of refractivity were measured in inversion layers. Using aircraft in controlled descending and ascending flights, Fukushima and Iriye (1964) found irregularities in refractivity exceeding 4 N units within 10 m in height. They also found middle-scale irregularities in the horizontal which they termed "refractivity clouds". These refractivity clouds were characterized by a median intensity of 2 N units and a median scale of 600 m. Clearly, atmospheric "fine" structure is such that the concept of a well defined horizontally homogeneous layer is often an over simplification.

Previous results of this study have concentrated on possible errors in atmospheric refractivity assessments caused by insufficient vertical resolution and by the assumptions of horizontal homogenity. The investigation into the effects of vertical resolution on duct detection suggests that the highest possible resolution is the most desirable. However, refraction variations in the ABL due to larger-scale turbulent eddies, as opposed to mean structure, could conceivably produce spurious ducts in an analysis if the data resolution is high enough. Organized structures, such as thermal plumes as first suggested by (Taylor, 1958), have been extensively investigated (e.g. Holland, 1968; Frisch and Businger, 1973; Khalsa and Businger, 1977; Lenschow and Stephens, 1980; Greenhut and Khalsa, 1982; Wilczak and Businger, 1983; and, Shaw and Businger, 1985). These investigations have shown significant variability in temperature and humidity, along with other atmospheric properties, between air inside and outside one of these features. Because the possibility of significant local variability in the atmospheric refractivity is real and could substantially affect IREPS analyses, some simple experiments using the CAPTEX and FASINEX data sets were conducted.

B. CAPTEX POTENTIAL LOCAL VARIABILITY

Table 6 is a numerical tabulation of microwave refractivity using both the mean and standard deviation values at selected levels derived from the 120 profiles taken

during the 47-day period of the CAPTEX experiment (Vaucher, 1986). In addition, two maximum deviation refractivity profiles were constructed by adding and subtracting half of the standard deviation values of refractivity from each of the mean values. A Monte-Carlo type experiment was designed such that six atmospheric profiles were constructed by randomly either using the value of mean N plus half of the standard deviation or the mean N minus half of the standard deviation for each level. Then, the resulting profiles were entered into the IREPS code to produce their corresponding atmospheric refractivity structure. Table 7 shows the results of some statistical manipulations performed upon the standard deviation derived profiles. Clearly, elevated ducting conditions are indicated quite frequently in the standard deviation-modified profiles whereas no ducts occurred from the use of the climatological mean profile.

C. FASINEX POTENTIAL LOCAL VARIABILITY

The previous experiment does not show the atmospheric variability associated with the intermittent larger scale-features. In order to investigate this possibility a second type of Monte-Carlo experiment was conceived. In this test, MABL properties reported in recent journal articles were applied to a typical FASINEX profile, which in turn, was input into the IREPS refractivity program to determine possible variations in MABL refractivity structure that could be caused by the path of a radiosonde going in and out of these larger-scale features existing in the MABL.

For all atmospheric temperatures, the second term and third terms of (2.3) can be combined so as to form (6.1) (Battan, 1973). This equation can be differentiated to determine the approximate effect of temperature and humidity variations on refractivity as shown in Equation 6.2.

$$N = 77.6\ P/T - 3.73 * 10^5\ e/T^2 \tag{6.1}$$

$$\Delta N = (\partial N/\partial q)\Delta q + (\partial N/\partial T)\Delta T \tag{6.2}$$

Shaw and Businger (1985) found that temperature variations in the open-ocean, extratropical MABL were insignificant (i.e. 0.05 deg C). However, humidity fluctuations were of sufficient magnitude to affect MABL refractivity. Using Air Mass

TABLE 6

CAPTEX MEAN AND STANDARD DEVIATION REFRACTIVITY VALUES FOR MICROWAVE PROPAGATION

HEIGHT (M)	MEAN N	σN	MEAN + σN/2	MEAN - σN/2
0	318.0	14.9	325.5	311.5
100	309.8	15.1	317.3	302.3
200	305.1	14.3	312.2	298.0
500	294.3	12.7	300.6	288.0
700	287.3	12.2	293.4	281.2
800	283.7	12.1	289.7	277.7
1000	275.5	12.7	281.8	269.2
1100	272.0	12.8	278.4	265.6
1200	268.2	13.3	274.8	261.6
1300	264.0	13.0	270.5	257.5
1400	260.1	13.4	266.8	253.4
1500	256.6	13.4	263.3	249.9
1700	248.3	13.7	255.1	241.5
1800	244.0	13.0	250.5	237.5
2000	236.8	12.5	243.0	230.6
2400	223.4	10.8	228.8	218.0
2700	214.50	9.72	219.36	209.64
2800	211.24	9.43	215.96	206.52
3000	206.41	9.22	211.02	201.80
3300	198.42	8.08	202.46	194.38
3500	193.62	7.88	197.56	189.68
3600	191.08	7.64	194.90	187.26
3800	185.93	6.80	189.33	182.53
4100	179.26	6.20	182.36	176.16
4900	162.66	4.37	164.85	160.48

TABLE 7

RESULTING STATISTICS FROM CAPTEX STANDARD DEVIATION DERIVED PROFILES

Average number of ducts per profile	2.2
Average thickness of the ducts (m)	117.5
Standard deviation of duct thickness (m)	20.2
Average strength of ducts (M Units)	2.5

Transformation Experiment (AMTEX) data, Lenschow and Stephens (1980) investigated the atmospheric structure of thermal versus non-thermal air in unusually convective regimes associated with cold air outbreaks over the Kuroshio current. Air inside these thermals can be identified by its upward vertical motion, humidity excess, and temperature excess (in the lower part of the MABL) when compared to air outside of a thermal. For refractivity calculations, increases in both temperature and humidity are compensating effects. Because we were interested in investigating a worst case scenario, we used information and equations from Lenschow and Stephens (1980) applied only to the humidity component of (6.2). Endeavor launch #1 was choosen as a typical FASINEX profile. The inversion layer height z_i was found by inspection to be approximately 1700 meters. (6.3) describes the humidity excess inside a thermal. Using an average value of m_* of 0.095 g/m^3 as a humidity scaling factor, and (6.4), which compares the temperature excess inside Θ_t and the temperature excess outside Θ_e a thermal, from Lenschow and Stephens (1980), (6.5) from (Fleagle and Businger, 1980), (6.6) and (6.7), and a modified equation of state, (6.8), the possible variations in refractivity, ΔN, due to possible humidity variations at each level were computed. Since the inversion layer caps the MABL, the levels above the inversion would not be affected by variations in the MABL. Hence, the upper levels of the profile were not modified in this experiment. Once the magnitude of ΔN for each layer was found, the layer was modified by $\pm \Delta N/2$ to simulate possible variations in refractivity that could occur as a radiosonde passed into and out of thermals. As done previously with the CAPTEX data, six experimental profiles were generated by randomly adding or subtracting the value of $\Delta N/2$ derived for each layer to the actual value of refractivity

for that layer. The resulting profiles were then entered into the IREPS 2.2 refraction code to see what effect, if any, would the intermittant larger-scale atmospheric features have on refractivity. Table 8 lists the resulting profiles which were subsequently used as input for IREPS.

$$q_t = m_* (1.8 (z/z_i)^{-1/3} *(1+2(z/z_i)^3)) \quad (6.3)$$

$$\Theta_e = -0.33\Theta_t \quad (6.4)$$

$$\log_{10} e_s = 11.4 - 2353/T \quad (6.5)$$

$$RH = e/e_s * 100 \quad (6.6)$$

$$q = .622\, e/P \quad (6.7)$$

$$P = \rho R_d T(1 + .61q) \quad (6.8)$$

The only effect on the control profile was to modify the already existing trapping layer in thickness by plus or minus 17 meters, 5%, and its strength of 22.2 M units by plus or minus 2.1 M units, 9%. In two of the six cases, a weak surface trapping layer, $dM/dz = -4\ Km^{-1}$, appeared where previously a near trapping layer, $dM/dz = 13.2\ Km^{-1}$, existed. The important result from this experiment is that temporary thermal-scale features in the MABL will have little effect on the mean refractive structure. Thus, spurious ducts from high-resolution measurements should not be a serious problem.

TABLE 8

MONTE-CARLO GENERATED N PROFILES FROM A TYPICAL FASINEX SOUNDING

LEVEL	CONTROL	TEST 1	TEST 2	TEST 3	TEST 4	TEST 5	TEST 6
1	343.0	343.0	343.0	343.0	343.0	343.0	343.0
2	328.9	330.7	327.2	330.7	330.7	327.2	330.7
3	322.3	323.6	323.6	323.6	323.6	323.6	321.1
4	321.0	319.9	319.9	322.1	322.1	322.1	322.1
5	312.4	313.5	311.4	311.4	313.5	311.4	311.4
6*	274.2	276.3	272.1	272.1	276.3	272.1	272.1

* Level 6 represents the top of the MABL

This same type of experiment was performed with the CAPTEX data. The temperature variation instead of the humidity variation term of Equation 6.2 was used for two reasons. First, humidity variations over land are generally smaller than humidity variations over water. Secondly, we wanted to compare the relative effects of humidity and temperature variations on refractivity. After applying the same procedure to a typical CAPTEX profile as was done previously with R/V Endeavor launch number one, we found virtually no effect on the control N profile from the surface to the ABL. Lane (1964) confirms this result by showing that fluctuations in humidity mixing-ratio have approximately a seven times greater effect on refractive index than do temperature fluctuations.

VII. SUMMARY AND CONCLUSIONS

IREPS version 2.2 is the newest refractive effects prediction system to be used by the Fleet. While it will provide important tactical information to operational commanders, the system will be limited in its ability to reflect the actual atmospheric refractive conditions by the quality and timeliness of the data which is currently used as input. By comparing the IREPS version 2.2 computed atmospheric refractivity conditions for a high resolution and degraded resolution sounding, we showed the importance of using high resolution data. The high resolution data were better able to define the smaller scale refractive structure of the atmosphere and, therefore, allowed IREPS to realistically portray the ambient ducting conditions.

The high resolution CAPTEX data also provided insight into how quickly atmospheric refractivity conditions can change. By observing the variabilty in ducting conditions for 120 soundings taken at irregular time intervals over a 47-day period, we found that refractive conditions are in constant dynamic evolution on diurnal as well as synoptic time scales. While refractive variability may not be as pronounced over water as it is over a continent, the implication that timely data must be used to achieve accurate refractivity condition predictions still should be considered by all IREPS users.

Although the IREPS version 2.2 user's manual implies horizontal inhomogeneity of the atmosphere should not be a serious refractivity consideration 85% of the time, the results of the investigations using the FASINEX data showed horizontal inhomogeneity does indeed cause significant variability in radar lobe coverage at least 50% of the time. This variability is not a function of ship separation distance, but appears to be driven by atmospheric conditions surrounding both platforms.

The last section of this thesis investigated the possibility of intermittently existing, relatively large-scale, atmospheric features creating spurious ducts because of the use of high resolution data. By applying worst case scenarios to our data base and entering modified sounding profiles into the IREPS version 2.2 refractivity code, we could compare the resulting output with the output of the original sounding. In both cases, with CAPTEX and FASINEX data, there was no significant modification of the previously existing refractive conditions. Accordingly, we see no disadvantages to using high resolution data. Quite to the contrary, we believe that only by the use of

timely, high resolution sounding data can an accurate assessment of atmospheric refractive conditions be derived by IREPS version 2.2.

LIST OF REFERENCES

Battan, L.J., 1973: *Radar Observation of the Atmosphere.* University of Chicago Press, 323 pp.

Bean, B.R., and E.J. Dutton, 1966: Radio Meteorology. *Radio Meteorology.* NBS Monagr 92. U.S. Department of Commerce, National Bureau of Standards, Washington. Dover, New York, 435 pp.

Davidson, K.L., 1986: Private communication

Ferber, J.F., and J.L. Heffter, 1983: *CAPTEX '83, Cross-Appalachian Tracer Experiments, Revised Plan,* National Oceanic and Atmospheric Administration Air Resources Laboratory, Rockville, Maryland, 22 pp.

Fleagle, R.G., and J.A. Businger, 1980: *An Introduction to Atmospheric Physics.* Second Ed., New York, Academic Press, 432 pp.

Frisch, A.S., and J.A. Businger, 1973: A Study of Convective Elements in the Atmosphere Surface Layer. *Bound.-Layer. Meteor.*, **3**, 301-328.

Fukushima, M., and H. Iriye, 1964: Preliminary Study of Spatial Distribution of Atmospheric Refractive Index from Aircraft Observations. *Proc. 1964 World Conf. on Radio. Meterorology*, Boulder, Colorado, 240-243.

Greenhut, G. and S.J.S. Khalsa, 1982: Updraft and Downdraft events in the Atmospheric Boundary layer over the Equatorial Pacific Ocean. *J. Atmos. Sci.*, 39, 1803-1818.

Halliday, D., and R. Resnick, 1981: *Fundamentals of Physics.* John Wiley and Sons, New York, 816 pp.

Holland, J.Z. 1968: An Application of some Statistical Techniques to the Study of Eddy Structure. U.S. Atomic Energy Commission Document TID-24585. 378 pp.

Kerr, D.E., 1951: *Propagation of Short Radio Waves.* McGraw-Hill, New York, 728 pp.

Khalsa, S.J.S, and J.A. Businger, 1977: The Drag Coefficient as Determined by the Dissipation Method and its relation to intermittent convection in the surface layer. *Bound.-Layer. Meteor.*, **12**, 273-297.

Lane, J.A., 1964: Some Measurements of the Structure of Elevated Layers in the Troposphere, *Proc. 1964 World Conf. on Radio. Meterorology*, Boulder, Colorado, 248-251.

Lenschow, D.H. and P.L. Stephens, 1980: The Role of Thermals in the Convective Boundary Layer. *Bound.-Layer Meteor.*, **19**, 509-532.

NOSC TD 659, 1981: *IREPS Revision 2.2 User's Manual*, Naval Ocean Systems Center, San Diego, California.

Shaw, W.J., and J.A. Businger, 1985: Intermittency and the Organization of Turbulence in the Near-Neutral Marine Atmospheric Boundary Layer. *J. Atmos. Sci.*, **42**, 2563-2584.

Stage, S.A. and R.A. Weller, 1985: The Frontal Air-Sea Interaction Experiment (FASINEX); Part I: Background and Scientific objectives. *Bull. Amer. Meteor. Soc.*, **66**, 1511-1520.

Stage, S.A and R.A. Weller, 1986: The Frontal Air-Sea Interaction Experiment (FASINEX); Part II: Experimental Plan. *Bull. Amer. Meteor. Soc.*, **67**, 16-20.

Stewart, R. W., 1979: *The Atmospheric Boundary Layer.* World Meteorological Organization No. 523, 44 pp.

Polmar, N., 1985: *The Ships and Aircraft of the U.S. Fleet.* U.S. Naval Institute. Arm and Armour Press, London, 559 pp.

Pollard, R. T., 1978: The Joint Air-Sea Interaction Experiment JASIN. *Bull. Amer. Meteor. Soc.*, **59**, 1310-1318.

Taylor, R.J., 1958: Thermal Structure in the lowest layers of the Atmosphere. *Aust. J. Phys. Meteor. Soc.*, **11**, 168-176.

Thomson, D.W., 1986: Private communication

Vaucher, C., 1986: Private communication

Webb, E.K., 1977: Convection Mechanisms of Atmospheric Heat Transfer from Surface to Global Scales, Second Australian Conference on Heat and Mass Transfer, Univesity of Sydney, 523-539.

Wilczak, J.M., and J.A. Businger, 1983: Thermally indirect motions in the convective Atmospheric Boundary Layer. *J. Atmos. Sci.*, **40**, 343-358.

Wyngaard, J.C., 1973: On Surface Layer Turbulence, Amer. Meteor. Soc., *Workshop on Micrometeorology*, D.A. Haugen, Ed., Boston, 101-148.

INITIAL DISTRIBUTION LIST

		No. Copies
1.	Defense Technical Information Center Cameron Station Alexandria, VA 22304-6145	2
2.	Library, Code 0142 Naval Postgraduate School Monterey, CA 93943-5002	2
3.	Chairman (Code 63Rd) Department of Meteorology Naval Postgraduate School Monterey, CA 93943-5000	1
4.	Chairman (Code 68Tm) Department of Oceanography Naval Postgraduate School Monterey, CA 93943-5000	1
5.	Professor W.J. Shaw (Code 63Sn) Department of Meteorology Naval Postgraduate School Monterey, CA 93943	2
6.	Professor D.W. Thomson Department of Meteorology Pennsylvania State University University Park, PA 16802	2
7.	Commander Naval Ocean Systems Command San Diego, CA 92152	1
8.	Director Naval Oceanography Division Naval Observatory 34th and Massachusetts Avenue NW Washington, DC 20390	1
9.	Commander Naval Oceanography Command NSTL Station Bay St. Louis, MS 39522	1
10.	Commanding Officer Naval Oceanographic Office NSTL Station Bay St. Louis, MS 39522	1

11.	Commanding Officer Fleet Numerical Oceanography Center Monterey, CA 93943-5000	1
12.	Commanding Officer Naval Ocean Research and Development Activity NSTL Station Bay St. Louis, MS 39522	1
13.	Commanding Officer Naval Environmental Prediction Research Facility Monterey, CA 93943-5000	1
14.	Chairman, Oceanography Department U.S. Naval Academy Annapolis, MD 21402	1
15.	Chief of Naval Research 800 N. Quincy Street Arlington, VA 22217	1
16.	Office of Naval Research (Code 420) Naval Ocean Research and Development Activity 800 N. Quincy Street Arlington, VA 22217	1
17.	Commanding Officer Naval Oceanography Command Center; Rota, Spain Box 31 FPO New York, NY 09450-3200	1
18.	Officer in Charge Naval Oceanography Command Detachment Monterey, CA 93943-5000	1
19.	Commanding Officer Space and Naval Warfare Systems Command NC #1 Code 3211K Washington D.C. 20363-5100	1
20.	Sharon L. LeVaugh 265 Mockingbird Lane Merritt Island, FL 32952	1
21.	LCDR Edward L. Dotson 2354 Rookery Way Va. Beach, VA 23445	1
22.	John Cook Naval Environmental Prediction Research Facility Monterey, CA 93943-5000	1

23.	Commander Naval Sea Systems Command Washington D.C. 20362	1
24.	Mr D. Britton Naval Sea Systems Command Attn: PMS 400B3B Washington D.C. 20362	1
25.	Mr James Schneider Surface Combat Systems John Hopkins University John Hopkins Road Laurel, MD 20707	1
26.	Chris Vaucher Department of Meteorology Naval Postgraduate School Monterey, CA 93943-5000	1

18767 3

DUDLEY KNOX LIBRARY
NAVAL POSTGRADUATE SCHOOL
MONTEREY, CALIFORNIA 93943-5002

Thesis
D6643 Dotson
c.1 An evaluation of the impact of variable temporal and spatial data resolution upon IREPS.

thesD6643
An evaluation of the impact of variable
3 2768 000 74985 7
DUDLEY KNOX LIBRARY